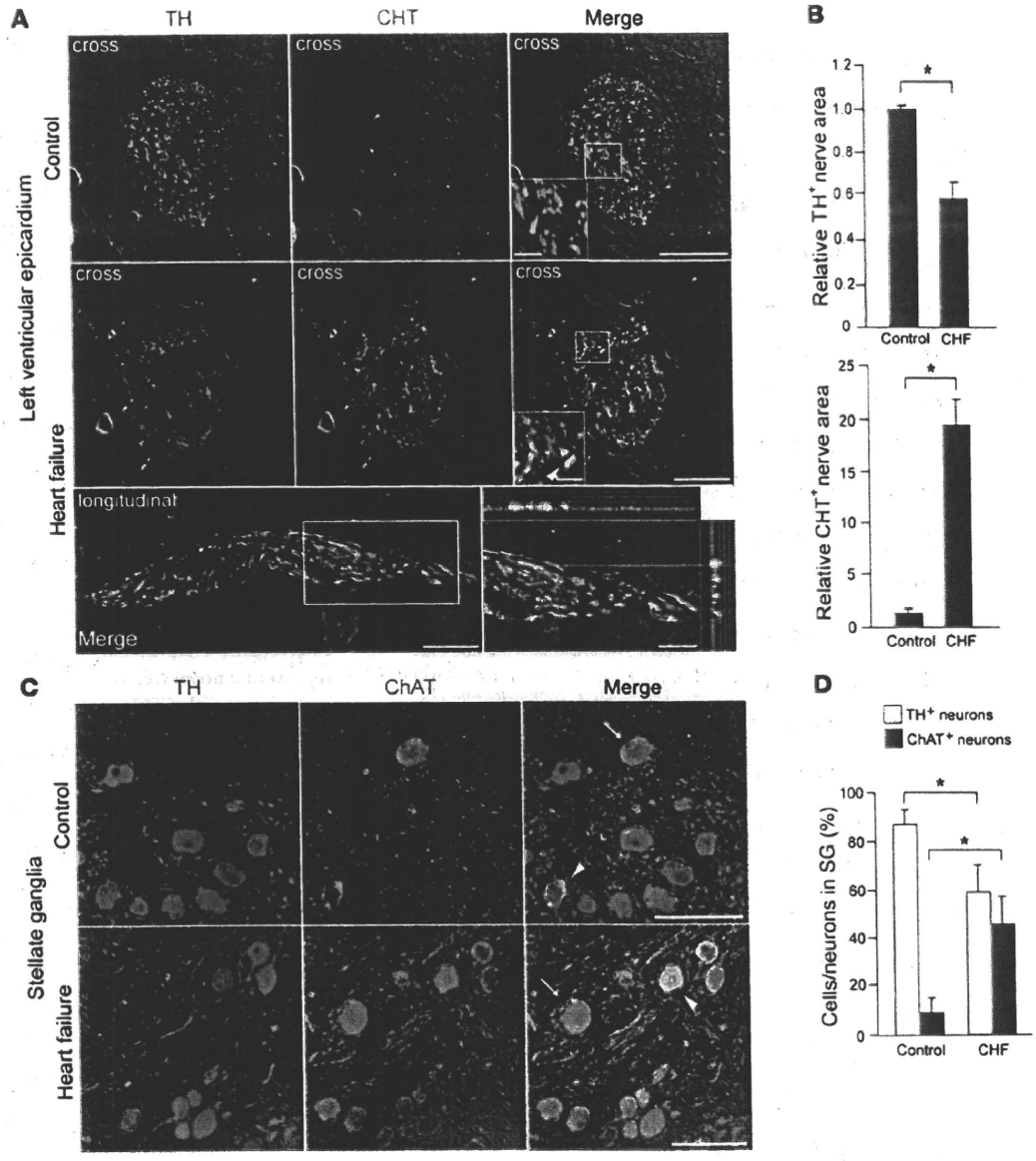

Figure 9

Neurotransmitter switching in the human cardiac sympathetic nervous system. (**A**) Representative immunostaining for TH (red) and CHT (green) in LVs at the epicardial sites in control and heart failure patients. Cross and longitudinal sections are shown. The longitudinal image is composed of 3 serial images. The heart failure group has fewer TH+ nerves and markedly more CHT+ nerves than the control group. In the ventricle of heart failure patients, some CHT+ nerves coexpress TH (arrowhead). The longitudinal section also revealed sympathetic nerves coexpressing TH and CHT. Higher-magnification views of the boxed regions are shown in the insets (right panels). (**B**) Quantitative analysis of TH+ and CHT+ nerve areas in LV ($n = 4$). (**C**) Representative immunostaining for TH (red) and ChAT (green) in the stellate ganglia of control and heart failure patients. Arrows indicate ChAT+ cells, and arrowheads indicate TH+/ChAT+ neurons. The heart failure group has fewer TH+ cells and more ChAT+ cells than the control group. (**D**) Quantification of TH+ and ChAT+ cells per total number of neurons in the stellate ganglia ($n = 5$). Representative data are shown in each panel. *$P < 0.01$. Scale bars: 10 μm (**A**, insets); 50 μm (**A** and inset in **D**); 100 μm (**C**).

lation, cardiomyocytes were cultured on laminin-coated silicon dishes that were stretched by 20% for 1 hour.

Lif and Ctf1 siRNA transfection. *Lif* and *Ctf1* siRNA and negative control (scrambled) siRNA were purchased from Ambion. Cardiomyocytes were transfected using the Lipofectamine RNAiMAX reagent (Invitrogen).

Culture of sympathetic neurons. Stellate ganglia neurons from 2-day-old Wistar rats (Japan CLEA) were dissociated and cultured in DMEM (Sigma-Aldrich) containing 5% fetal bovine serum and nerve growth factor (50 ng/ml; Upstate), as described previously (8, 9). Proliferation of non-neuronal cells was prevented by addition of 10 μM cytosine 1β-D-arabino furanoside (Sigma-Aldrich) for the first 5 days. After 2 days, the neurons were cultured with LIF (Chemicon) or cardiomyocyte-conditioned media for 14 days. The culture media was replaced every 2–3 days.

RNA extraction and quantitative RT-PCR. RNA extraction and quantitative RT-PCR were performed as described previously (45) using the ABI Prism 7500 Sequence Detection System (Applied Biosystems). All samples were

run in triplicate. The primers and TaqMan probe for LIF (Rn00573491_g1, Mm00434762_g1), CT-1 (Rn00567503_m1, Mm00432772_m1), ciliary neurotrophic factor (Rn00755092_m1), cardiotrophin-like cytokine (Rn02133709_s1), nerve growth factor (Rn02133709_s1), brain-derived neurotrophic factor (Rn01484928_m1), neurotrophin-3 (Rn00579280_m1), GDNF (Rn00569510_m1), VAChT (Rn00581454_s1), CHT (Rn00506029_m1), TH (Rn00562500_m1), brain natriuretic peptide (Rn00580641_m1, Mm00435304_g1), angiotensinogen (Rn00593114_m1), and ACE (Rn00561094_m1) were purchased from Applied Biosystems. The mRNA levels were normalized by comparison to GAPDH.

RT-PCR. The primers for ChAT (46) and VAChT (47) were as described previously. The primers for murine LIF were murine LIF forward, 5′-CCTCTAGAGTCCAGCCCATAA-3′, and murine LIF reverse, 5′-CTCTAGAAGGCCTGGACCAC-3′.

Western blot analysis. Samples were prepared by homogenization of hearts in ice-cold buffer as described (45). Immunodetection was performed with an anti-LIF antibody (AB-449-NA; R&D Systems). After transfer to nitrocellulose membranes, LIF protein was visualized by chemiluminescence detection (SuperSignal West Pico; Pierce).

Immunohistochemistry. Hearts were perfused from the apex with 0.4% paraformaldehyde in PBS, fixed overnight, embedded in OCT compound, and then frozen in liquid nitrogen. Cryostat sections were stained with antibodies against TH (Chemicon, Sigma-Aldrich, and ImmunoStar) and DBH to detect sympathetic nerves, with CHT (Chemicon) and ChAT (Chemicon) to detect parasympathetic nerves, and with calcitonin gene-related peptide (Biogenesis) to detect sensory nerves. The sections were incubated with secondary antibodies conjugated with Alexa Fluor 488, Alexa Fluor 546, Alexa Fluor 633 (Molecular Probes) and TRITC (DAKO), and the nuclei were stained with Toto3 (Molecular Probes). All confocal microscopy was carried out on a LSM 510 META Confocal Microscope (Carl Zeiss). In some experiments, paraffin-embedded sections were treated with 10 mM citrate buffer (pH 6) and 20 mM Tris-HCL buffer (pH 9) for antigen retrieval, and signals were visualized using a TSA Direct Kit (NEN Life Science). Nerve density was determined using ImageJ software (http://rsbweb.nih.gov/ij/) (48). For human sympathetic ganglia, cresyl violet staining (Nissl staining) was performed, and the total number of neurons was determined.

Anterograde labeling of sympathetic nerve fibers. To label sympathetic nerve fibers in the stellate ganglia, DS and DR rats were injected with 10% BDA in the left stellate ganglia, via a Hamilton micropipette under mechanical ventilation. The rats were killed after 3 days and were perfused with 0.4% paraformaldehyde in PBS for immunohistochemistry.

Transmission electron microscopy. Hearts were fixed with 0.2% glutaraldehyde and 0.4% paraformaldehyde in 0.1 M cacodylate buffer and embedded in epoxy resin. Ultrathin sections (80 nm) were stained as described previously (49) and viewed under a JEOL-1230 transmission electron microscope (JEOL Ltd.). AF64A was prepared from acetylethylcholine mustard hydrochloride (Sigma-Aldrich) and administered to rats intraperitoneally (150 μmol/kg). AF64A is specifically taken up by CHT and degenerates cholinergic nerve fibers. Saline was injected in control experiments. After 3 days, hearts were removed and fixed as above. The samples were immunostained with an antibody against TH (Chemicon) and incubated with a secondary antibody of Nanogold-Fab conjugates (Nanoprobes). The conjugated gold particles were visualized as described previously (50).

Mouse models of heart failure. LV failure was induced by TAC, which was performed by ligating the transverse thoracic aorta with a 27-gauge needle, using a 7.0 nylon suture (51). RV failure was induced by long-standing hypoxia (10% O_2) in the mouse model of pulmonary hypertension as described previously (52).

Echocardiography and hemodynamic measurements. Transthoracic echocardiography was performed with a Vevo 770 scanner (VisualSonics), using 17.5 and 30 MHz probes. TAC pressure gradients were determined by pulsed-wave Doppler echocardiography and calculated as $4 \times V_{max}^2$, where V_{max} is the velocity of the blood across the constriction. Mice with a pressure gradient of more than 40 mmHg were included in the study. For hemodynamic measurements, the mice were intubated and then mechanically ventilated with a respirator. A left thoracotomy was performed, and RV pressure was measured from a 1.0F Mikro-Tip pressure transducer (SPR-1000; Millar Instruments), directly inserted into the RV. The LV and aortic pressures were measured by catheters inserted into the right carotid artery. LV pressure, RV pressure, and aortic pressure were recorded using a polygraph system (iWorx Systems Inc.). All recordings were performed on rats and mice anesthetized with 2% isoflurane.

Human samples. Control samples of LV and stellate ganglia were prepared from 8 autopsied patients without heart disease (mean age, 57 ± 17 years). Heart failure samples were prepared from 8 autopsied patients (mean age, 51 ± 13 years), who died of CHF due to various heart diseases, as described in Table 1. After removal samples were fixed immediately in 0.4% paraformaldehyde and embedded in paraffin or OCT compound. The use of autopsied specimens of human tissue was approved by the institutional review board of Keio University and National Cardiovascular Center.

Statistics. Values are presented as mean ± SD. Statistical significance was evaluated using 2-tailed, unpaired Student's *t* tests for comparisons of 2 mean values. *P* values of less than 0.05 were considered statistically significant. Kaplan-Meier survival curves were analyzed by SPSS software. Survival analysis was performed by using the Kaplan-Meier method. The log-rank test was used to compare survival curves.

Acknowledgments

We thank Yoshiko Miyake, Yoko Shiozawa, Seiichi Kotoda, Yoshiharu Tsuru, Toshihiro Nagai, Koji Shimoda, and Toshio Terashima for excellent technical assistance. We are also grateful to Kazuto Yamazaki, Keiko Fukada, and Takeshi Suzuki for their comments on the manuscript. This study was supported in part by research grants from the Ministry of Education, Science and Culture, Japan, and by the Program for Promotion of Fundamental Studies in Health Science of the National Institute of Biomedical Innovation (to K. Fukuda).

Received for publication May 6, 2009, and accepted in revised form November 11, 2009.

Address correspondence to: Keiichi Fukuda, Department of Regenerative Medicine and Advanced Cardiac Therapeutics, Keio University School of Medicine, 35 Shinanomachi, Shinjuku-ku, Tokyo 160-8582, Japan. Phone: 81-3-5363-3874; Fax: 81-3-5363-3875; E-mail: kfukuda@sc.itc.keio.ac.jp.

1. Cao JM, et al. Relationship between regional cardiac hyperinnervation and ventricular arrhythmia. *Circulation.* 2000;101(16):1960–1969.
2. Bristow MR, et al. Beta-adrenergic neuroeffector abnormalities in the failing human heart are produced by local rather than systemic mechanisms. *J Clin Invest.* 1992;89(3):803–815.
3. Chidsey CA, Kaiser GA, Sonnenblick EH, Spann JF, Braunwald E. Cardiac norephinephrine stores in experimental heart failure in the dog. *J Clin Invest.* 1964;43:2386–2393.
4. Backs J, et al. The neuronal norepinephrine transporter in experimental heart failure: evidence for a posttranscriptional downregulation. *J Mol Cell Cardiol.* 2001;33(3):461–472.
5. Himura Y, et al. Cardiac noradrenergic nerve terminal abnormalities in dogs with experimental congestive heart failure. *Circulation.* 1993;88(3):1299–1309.
6. Kimura K, et al. Cardiac Sympathetic Rejuvenation: A Link between Nerve Function and Cardiac Hypertrophy. *Circ Res.* 2007;100(12):1755–1764.
7. Francis NJ, Landis SC. Cellular and molecular determinants of sympathetic neuron development. *Annu Rev Neurosci.* 1999;22:541–566.

8. Patterson PH, Chun LL. The influence of non-neuronal cells on catecholamine and acetylcholine synthesis and accumulation in cultures of dissociated sympathetic neurons. *Proc Natl Acad Sci U S A.* 1974;71(9):3607–3610.
9. Fukada K. Hormonal control of neurotransmitter choice in sympathetic neurone cultures. *Nature.* 1980;287(5782):553–555.
10. Fukada K. Purification and partial characterization of a cholinergic neuronal differentiation factor. *Proc Natl Acad Sci U S A.* 1985;82(24):8795–8799.
11. Yamamori T, et al. The cholinergic neuronal differentiation factor from heart cells is identical to leukemia inhibitory factor. *Science.* 1989; 246(4936):1412–1416.
12. Stanke M, et al. Target-dependent specification of the neurotransmitter phenotype: cholinergic differentiation of sympathetic neurons is mediated in vivo by gp 130 signaling. *Development.* 2006; 133(1):141–150.
13. Bamber BA, Masters BA, Hoyle GW, Brinster RL, Palmiter RD. Leukemia inhibitory factor induces neurotransmitter switching in transgenic mice. *Proc Natl Acad Sci U S A.* 1994;91(17):7839–7843.
14. Blum A, Miller H. Role of cytokines in heart failure. *Am Heart J.* 1998;135(2 Pt 1):181–186.
15. Hirota H, et al. Circulating interleukin-6 family cytokines and their receptors in patients with congestive heart failure. *Heart Vessels.* 2004;19(5):237–241.
16. MacGowan GA, Mann DL, Kormos RL, Feldman AM, Murali S. Circulating interleukin-6 in severe heart failure. *Am J Cardiol.* 1997;79(8):1128–1131.
17. Ieda M, et al. Sema3a maintains normal heart rhythm through sympathetic innervation patterning. *Nat Med.* 2007;13(5):604–612.
18. Potter DD, Landis SC, Matsumoto SG, Furshpan EJ. Synaptic functions in rat sympathetic neurons in microcultures. II. Adrenergic/cholinergic dual status and plasticity. *J Neurosci.* 1986;6(4):1080–1098.
19. Fisher A, Mantione CR, Abraham DJ, Hanin I. Long-term central cholinergic hypofunction induced in mice by ethylcholine aziridinium ion (AF64A) in vivo. *J Pharmacol Exp Ther.* 1982;222(1):140–145.
20. Zigmond RE, et al. Phenotypic plasticity in adult sympathetic neurons: changes in neuropeptide expression in organ culture. *Proc Natl Acad Sci U S A.* 1992;89(4):1507–1511.
21. Furshpan EJ, Landis SC, Matsumoto SG, Potter DD. Synaptic functions in rat sympathetic neurons in microcultures. I. Secretion of norepinephrine and acetylcholine. *J Neurosci.* 1986;6(4):1061–1079.
22. Delree P, et al. Plasticity of developing and adult dorsal root ganglion neurons as revealed in vitro. *Brain Res Bull.* 1993;30(3–4):231–237.
23. Hasking GJ, et al. Norepinephrine spillover to plasma in patients with congestive heart failure: evidence of increased overall and cardiorenal sympathetic nervous activity. *Circulation.* 1986;73(4):615–621.
24. Meredith IT, et al. Cardiac sympathetic nervous activity in congestive heart failure. Evidence for increased neuronal norepinephrine release and preserved neuronal uptake. *Circulation.* 1993; 88(1):136–145.
25. Merlet P, et al. Prognostic value of cardiac metaiodobenzylguanidine imaging in patients with heart failure. *J Nucl Med.* 1992;33(4):471–477.
26. Henderson EB, et al. Abnormal I-123 metaiodobenzylguanidine myocardial washout and distribution may reflect myocardial adrenergic derangement in patients with congestive cardiomyopathy. *Circulation.* 1988;78(5 Pt 1):1192–1199.
27. Qin F, Vulapalli RS, Stevens SY, Liang CS. Loss of cardiac sympathetic neurotransmitters in heart failure and NE infusion is associated with reduced NGF. *Am J Physiol Heart Circ Physiol.* 2002; 282(1):H363–H371.
28. Kaye DM, Vaddadi G, Gruskin SL, Du XJ, Esler MD. Reduced myocardial nerve growth factor expression in human and experimental heart failure. *Circ Res.* 2000;86(7):E80–E84.
29. Schmid P G, et al. Selective sympathetic neural changes in hypertrophied right ventricle. *Am J Physiol.* 1982;243(2):H175–H180.
30. Liang CS, Yatani A, Himura Y, Kashiki M, Stevens SY. Desipramine attenuates loss of cardiac sympathetic neurotransmitters produced by congestive heart failure and NE infusion. *Am J Physiol Heart Circ Physiol.* 2003;284(5):H1729–H736.
31. Wang H, Lu Y, Wang Z. Function of cardiac M3 receptors. *Auton Autacoid Pharmacol.* 2007;27(1):1–11.
32. LaCroix C, Freeling J, Giles A, Wess J, Li YF. Deficiency of M2 muscarinic acetylcholine receptors increases susceptibility of ventricular function to chronic adrenergic stress. *Am J Physiol Heart Circ Physiol.* 2008;294(2):H810–H820.
33. Li M, et al. Vagal nerve stimulation markedly improves long-term survival after chronic heart failure in rats. *Circulation.* 2004;109(1):120–124.
34. Rao MS, et al. Leukemia inhibitory factor mediates an injury response but not a target-directed developmental transmitter switch in sympathetic neurons. *Neuron.* 1993;11(6):1175–1185.
35. Berry MF, et al. Targeted overexpression of leukemia inhibitory factor to preserve myocardium in a rat model of postinfarction heart failure. *J Thorac Cardiovasc Surg.* 2004;128(6):866–875.
36. Brodski C, Schnurch H, Dechant G. Neurotrophin-3 promotes the cholinergic differentiation of sympathetic neurons. *Proc Natl Acad Sci U S A.* 2000;97(17):9683–9688.
37. Brodski C, Schaubmar A, Dechant G. Opposing functions of GDNF and NGF in the development of cholinergic and noradrenergic sympathetic neurons. *Mol Cell Neurosci.* 2002;19(4):528–538.
38. Jougasaki M, et al. Leukemia inhibitory factor is augmented in the heart in experimental heart failure. *Eur J Heart Fail.* 2003;5(2):137–145.
39. Eiken HG, et al. Myocardial gene expression of leukaemia inhibitory factor, interleukin-6 and glycoprotein 130 in end-stage human heart failure. *Eur J Clin Invest.* 2001;31(5):389–397.
40. Kanegae Y, et al. Efficient gene activation system on mammalian cell chromosomes using recombinant adenovirus producing Cre recombinase. *Gene.* 1996;181(1–2):207–212.
41. Agah R, et al. Gene recombination in postmitotic cells: targeted expression of Cre recombinase provokes cardiac-restricted, site-specific rearrangement in adult ventricular muscle in vivo. *J Clin Invest.* 1997;100(1):169–179.
42. Betz UA, et al. Postnatally induced inactivation of gp130 in mice results in neurological, cardiac, hematopoietic, immunological, hepatic, and pulmonary defects. *J Exp Med.* 1998;188(10):1955–1965.
43. Parlato R, Otto C, Begus Y, Stotz S, Schütz G. Specific ablation of the transcription factor CREB in sympathetic neurons surprisingly protects against developmentally regulated apoptosis. *Development.* 2007;134(9):1663–1670.
44. Kawamoto S, et al. A novel reporter mouse strain that expresses enhanced green fluorescent protein upon Cre-mediated recombination. *FEBS Lett.* 2000;470(3):263–268.
45. Ieda M, et al. Endothelin-1 regulates cardiac sympathetic innervation in the rodent heart by controlling nerve growth factor expression. *J Clin Invest.* 2004;113(6):876–884.
46. Fann MJ, Patterson PH. A novel approach to screen for cytokine effects on neuronal gene expression. *J Neurochem.* 1993;61(4):1349–1355.
47. Berrard S, et al. Coregulation of two embedded gene products, choline acetyltransferase and the vesicular acetylcholine transporter. *J Neurochem.* 1995; 65(2):939–942.
48. Ieda M, et al. Nerve growth factor is critical for cardiac sensory innervation and rescues neuropathy in diabetic hearts. *Circulation.* 2006;114(22):2351–2363.
49. Yamazaki K, Eyden BP. Gap junctions and nerve terminals among stromal cells in human fallopian tube ampullary mucosa. *J Submicrosc Cytol Pathol.* 1998;30(3):399–408.
50. Nakata K, Okuda T, Misawa H. Ultrastructural localization of high-affinity choline transporter in the rat neuromuscular junction: enrichment on synaptic vesicles. *Synapse.* 2004;53(1):53–56.
51. Rockman HA, et al. Segregation of atrial-specific and inducible expression of an atrial natriuretic factor transgene in an in vivo murine model of cardiac hypertrophy. *Proc Natl Acad Sci U S A.* 1991; 88(18):8277–8281.
52. Endo J, et al. BM-derived cells contribute to the pathogenesis of cardiac hypertrophy in response to pressure overload. *Circulation.* 2007;116(10):1176–1184.

Journal of Molecular and Cellular Cardiology 49 (2010) 576–586

Contents lists available at ScienceDirect

Journal of Molecular and Cellular Cardiology

journal homepage: www.elsevier.com/locate/yjmcc

Original article

4-Hydroxy-2-nonenal protects against cardiac ischemia–reperfusion injury *via* the Nrf2-dependent pathway

Yan Zhang [a,1], Motoaki Sano [a,d,*], Ken Shinmura [b], Kayoko Tamaki [b], Yoshinori Katsumata [a], Tomohiro Matsuhashi [a], Shintaro Morizane [a], Hideyuki Ito [a], Takako Hishiki [c], Jin Endo [a], Heping Zhou [a], Shinsuke Yuasa [a], Ruri Kaneda [a], Makoto Suematsu [c], Keiichi Fukuda [a]

[a] Department of Cardiology, Keio University School of Medicine, Tokyo, 160-8582, Japan
[b] Department of Geriatric Medicine, Keio University School of Medicine, Tokyo, 160-8582, Japan
[c] Department of Biochemistry and Integrative Medical Biology, Keio University School of Medicine, Tokyo, 160-8582, Japan
[d] Precursory Research for Embryonic Science and Technology (PRESTO), Japan Science and Technology Agency, Saitama, 332-0012, Japan

ARTICLE INFO

Article history:
Received 25 December 2009
Received in revised form 24 April 2010
Accepted 21 May 2010
Available online 4 June 2010

Keywords:
4-Hydroxy-2-nonenal
Ischemia–reperfusion injury
Nrf2
Hormesis
Glutathione

ABSTRACT

Reactive oxygen species (ROS) attack polyunsaturated fatty acids of the membrane and trigger lipid peroxidation, which results in the generation of α,β-unsaturated aldehydes, such as 4-hydroxy-2-nonenal (4-HNE). There is compelling evidence that high concentrations of aldehydes are responsible for much of the damage elicited by cardiac ischemia–reperfusion injury, while sublethal concentrations of aldehydes stimulate stress resistance pathways, to achieve cardioprotection. We investigated the mechanism of cardioprotection mediated by 4-HNE. For cultured cardiomyocytes, 4-HNE was cytotoxic at higher concentrations (≥20 μM) but had no appreciable cytotoxicity at lower concentrations. Notably, a sublethal concentration (5 μM) of 4-HNE primed cardiomyocytes to become resistant to cytotoxic concentrations of 4-HNE. 4-HNE induced nuclear translocation of transcription factor NF-E2-related factor 2 (Nrf2), and enhanced the expression of γ-glutamylcysteine ligase (GCL) and the core subunit of the Xc^- high-affinity cystine transporter (xCT), thereby increasing 1.45-fold the intracellular GSH levels. Cardiomyocytes treated with either Nrf2-specific siRNA or the GCL inhibitor L-buthionine sulfoximine (BSO) were less tolerant to 4-HNE. Moreover, the cardioprotective effect of 4-HNE pretreatment against subsequent glucose-free anoxia followed by reoxygenation was completely abolished in these cells. Intravenous administration of 4-HNE (4 mg/kg) activated Nrf2 in the heart and increased the intramyocardial GSH content, and consequently improved the functional recovery of the left ventricle following ischemia–reperfusion in Langendorff-perfused hearts. This cardioprotective effect of 4-HNE was not observed for Nrf2-knockout mice. In summary, 4-HNE activates Nrf2-mediated gene expression and stimulates GSH biosynthesis, thereby conferring on cardiomyocytes protection against ischemia–reperfusion injury.

1. Introduction

Reactive oxygen species (ROS) originate from various sources, including the Nox family of NADPH oxidases, xanthine oxidase, and mitochondria, in which superoxide radicals are the byproducts of oxidative energy production. Superoxide radicals are dismuted by superoxide dismutase (SOD), to produce hydrogen peroxides, which in turn are degraded into water and molecular oxygen by catalase, glutathione peroxidase (Gpx), and peroxiredoxin (Prx). Hydroxyl radicals (OH•), which are the most potent ROS, are formed from hydrogen peroxides through the Fenton reaction. No endogenous enzymes exist to eliminate these radicals. The OH• attack neighboring polyunsaturated fatty acids in the cell membrane, thereby triggering lipid peroxidation, which results in the generation of lipid hydroperoxides and α,β-unsaturated aldehydes, including 4-hydroxy-2-nonenal (4-HNE). These aldehydes are highly electrophilic and react with biomolecules, such as proteins and nucleic acids, to generate various adducts [1]. By virtue of their high chemical stability, these lipid peroxidation products diffuse greater distances than their precursor ROS, so they can disseminate oxidative injury and amplify damage. Aldehydes accumulation is found in ischemic, hypertrophic, and failing hearts, as well as in the oxidation of LDL [2], atherosclerotic lesions, and the brains of patients with Alzheimer's disease [3], and therefore, have been implicated in the pathogenesis of oxidative stress-associated diseases. Pretreatment with a small molecule activator of an aldehyde-detoxifying enzyme, aldehyde dehydrogenase 2

* Corresponding author. Department of Cardiology, Keio University School of Medicine, 35 Shinanomachi Shinjuku-ku, Tokyo, 160-8582, Japan. Tel.: +81 3 5363 3874; fax: +81 3 5363 3875.
E-mail address: msano@sc.itc.keio.ac.jp (M. Sano).
[1] Present address: Department of Pharmacology, Harbin Medical University, Harbin, China.

0022-2828/$ – see front matter © 2010 Elsevier Ltd. All rights reserved.
doi:10.1016/j.yjmcc.2010.05.011

(ALDH2), reduced infarct size by 60% in a rat model of ischemia–reperfusion injury [4], which indicates that much of the damage inflicted by ischemia–reperfusion is attributable to aldehydes generated in the ischemic heart.

Although the pathogenic effects of ROS are well established, antioxidant supplements for the prevention of cardiovascular events have been found to lack efficacy, and may even be harmful [5]. This discrepancy may be attributable to the dual role of ROS. ROS are not simply toxic byproducts, since they also play important roles in establishing antioxidant defense mechanisms. The sensing of aldehyde accumulation in injured tissues enables the cell to activate a variety of stress resistance pathways in a cell-type-specific manner, so as to counteract oxidative stress-mediated injury [6–8]. This induction of protective mechanisms by stressors is referred to as "stress-response hormesis" [9]. Therefore, aldehydes may be regarded as second messengers that propagate ROS-initiating favorable signaling.

In the present study, we investigated whether 4-HNE, which is one of the most abundant aldehydes produced by lipid peroxidation *in vivo*, induces stress-response hormesis in cultured cardiomyocytes and in *in vivo* hearts, and determined the underlying mechanisms.

2. Materials and methods

2.1. Animals

All animal experiments were reviewed and approved by the Institutional Animal Care and Use Committee at Keio University School of Medicine. Male C57BL/6 J mice at 10 weeks of age were obtained from CLEA Japan (Tokyo, Japan). Nrf2-knockout mice on a C57BL/6 J background were generated as previously described [10]. For comparison, Nrf2-wildtype mice (C57BL/6 J) were obtained from siblings of the Nrf2-knockout.

2.2. Cell culturing

Neonatal ventricular myocytes from 1- to 2-day-old Sprague–Dawley rats were subjected to Percoll gradient centrifugation and differential plating, to enrich for cardiac myocytes and to deplete non-myocytes [11]. Cell viability was determined using the LIVE/DEAD Viability/Cytotoxicity Assay Kit (Molecular Probes), which is based on the simultaneous determination of live and dead cells with the calcein AM and ethidium homodimer-1 probes, which are specific for intracellular esterase activity and membrane integrity, respectively. Fluorescence imaging of the cells (live cells were labeled green, whereas the nuclei of dead cells were labeled red) was performed with a fluorescence microscope (BZ-9000; Keyence).

2.3. Western blotting

Nuclear extracts were prepared as described previously [11]. The following rabbit polyclonal antibodies were used: anti-Nrf2 and anti-xCT (core subunit of the Xc^- high-affinity cystine transporter) (Santa Cruz Biotechnology); anti-HO1 (hemoxygenase-1), (Stressgen); anti-catalase and anti-Gclc (catalytic subunit of γ-glutamylcysteine ligase) (Abcam); anti-Gsta2 (glutathione-S-transferase A2) (Novus Biologicals); anti-4-HNE adduct (Calbiochem). Immunoreactive proteins were visualized using horseradish peroxidase-conjugated secondary antibodies, enhanced chemiluminescence (Amersham Biosciences), and the LAS-3000 luminoimager (Fujifilm).

2.4. Quantitative Real-Time PCR

Total RNA samples from cultured cardiomyocytes and hearts were prepared using the Trizol reagent (Invitrogen), according to manufacturer's instructions. Samples of total RNA (2 μg) were reverse-transcribed using the RNA PCR Kit (Takara Biotechnology, Japan), and the resulting cDNA was used as a PCR template. The mRNA levels were determined by Real-Time PCR with the ABI PRISM 7700 Sequence Detector (Applied Biosystems), according to the manufacturer's instructions. Predesigned gene-specific primer and probe sets (TaqMan Gene Expression Assays) were used. The 18s ribosomal RNA was amplified as an internal control. The relative gene expression level (the amount of target, normalized to the endogenous control gene) was calculated using the comparative Ct method formula: $2^{-\Delta\Delta Ct}$.

2.5. siRNA oligonucleotides and transfection

The siRNA oligonucleotides directed against the rat Nrf2 and a control siRNA (Ambion) were transfected into cells using the Lipofectamine RNAiMAX reagent (Invitrogen) .

2.6. Determination of intracellular glutathione concentration

The intracellular concentration of GSH was measured spectrophotometrically (U-2810 spectrophotometer; Hitachi) using the Bioxytech GSH/GSSG-412 kit (Oxis Research), according to the manufacturer's instructions. All assays were performed in triplicate on at least three separate occasions.

2.7. Langendorff perfusion of the heart

Hearts were excised rapidly from heparinized mice, perfused with modified Krebs–Henseleit buffer (120 mmol/L NaCl, 25 mmol/L $NaHCO_3$, 5.9 mmol/L KCl, 1.2 mmol/L $MgSO_4$, 1.75 mmol/L $CaCl_2$, and 10 mmol/L glucose), and gassed with 95% O_2 and 5% CO_2 at 37 °C according to the Langendorff procedure. Coronary perfusion pressure was maintained at 90 mm Hg. A plastic catheter with a polyethylene balloon was inserted into the left ventricle (LV) through the left atrium. Before the induction of ischemia, the left ventricular end-diastolic pressure was adjusted to 10 mm Hg by filling the balloon with water. The indices of LV function, including LV systolic pressure (LVSP), LV end-diastolic pressure (LVEDP), and positive dP/dt, were recorded as described previously. The total lactate dehydrogenase (LDH) activity released into the perfusate was measured with a commercially available kit (Sigma) [11]. To examine the effect of 4-HNE treatment on function recovery after ischemia–reperfusion, mice were injected with either 4 mg/kg 4-HNE or vehicle (50 μl of saline) *via* the retro-orbital vein [12] [13]. The efficacy of injection via the retro-orbital vein was confirmed using Evans Blue (Supplemental Fig. 1).

2.8. Statistical analysis

The values are presented as mean ± SEM. Statistical significance was evaluated using 2-tailed, unpaired Student's *t*-tests for comparisons of two mean values. Multiple comparisons involving more than three groups were performed using ANOVA. A *P*-value less than 0.05 was considered statistically significant.

3. Results

3.1. High-dosage 4-HNE causes cardiomyocyte cell death

Neonatal rat cardiomyocytes were treated with various concentrations of 4-HNE for 24 h, and 4-HNE-induced cardiomyocyte toxicity was monitored (Fig. 1A, B). The viabilities of the cardiomyocytes in the presence of 0, 5, 10, 20, and 40 μM 4-HNE were 82.17% ± 3.19%, 80.96% ± 2.76%, 72.85% ± 2.06%, 28.95% ± 3.54%, and 0.00%, respectively (Fig. 1A). At concentrations >20 μM, HNE significantly decreased cell viability, whereas 5 μM or 10 μM 4-HNE showed no appreciable cytotoxicity. Based on these observations, concentrations of 4-HNE < 10 μM were selected for subsequent studies on the potential favorable effects of 4-HNE.

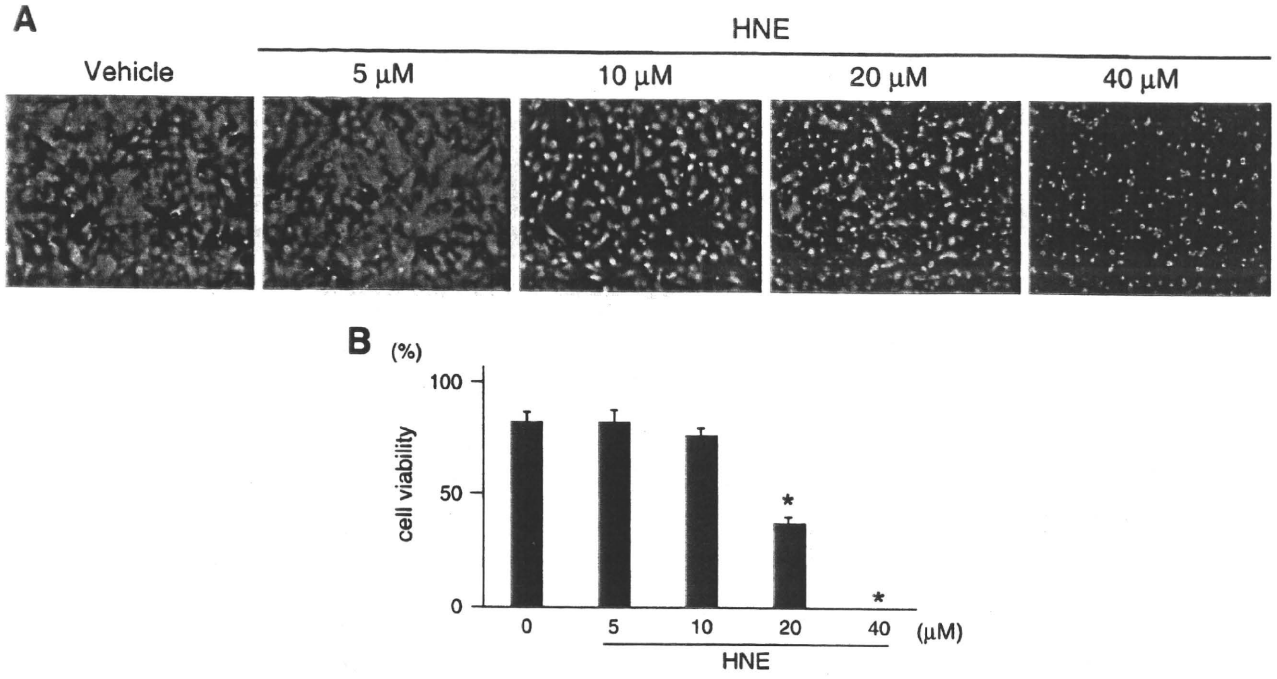

Fig. 1. 4-HNE causes cell death at higher concentrations but lacks cytotoxicity at lower concentrations. (A) Representative images of cardiomyocytes that were treated with different concentrations of 4-HNE. (B) Quantification of cell viability. Data shown are mean ± SEM ($n = 5$). *$P<0.05$ vs. vehicle-treated cardiomyocytes (unpaired Student's t-test).

3.2. Pretreatment with a sublethal concentration of 4-HNE protects cardiomyocytes against subsequent oxidative cell death induced by a high dosage of 4-HNE

To examine the effects of 4-HNE, cardiomyocytes were pretreated with either vehicle or 5 μM 4-HNE for 14 h, and then treated with cytotoxic concentrations of 4-HNE for 24 h. The viabilities of the vehicle-pretreated cardiomyocytes were 24.59% ± 4.31% for 20 μM 4-HNE and 15.42% ± 1.76% for 30 μM 4-HNE. Pretreatment with 5 μM 4-HNE significantly increased the cardiomyocyte viabilities to 72.09% ± 5.53% for 20 μM 4-HNE and 38.65% ± 4.12% for 30 μM 4-HNE (Fig. 2A, B).

3.3. 4-HNE induces antioxidant enzymes and GSH synthesis in cardiomyocytes

We examined the underlying molecular mechanisms responsible for the cytoprotective effect of 4-HNE on cardiomyocytes. 4-HNE treatment increased both the mRNA and protein expression levels of various antioxidant enzymes, including HO-1, catalase, Gsta2, Gclc, and xCT (Fig. 3A, B). The rate of glutathione (GSH) synthesis is determined primarily by Gclc activity and the availability of precursor amino acids, especially cysteine. Consistent with the increased levels of Gclc and xCT, the intracellular concentration of GSH was increased 1.45-fold in cardiomyocytes that were treated with 5 μM 4-HNE for 24 h, as compared to cells that were treated with vehicle (261.08 ± 19.35 μM/g vs. 179.89 ± 11.59 μM/g, respectively) (Fig. 3C).

3.4. Nrf2 plays a key role in the induction of stress responses

Nrf2 has been implicated as a key transcription factor that induces the expression of antioxidant genes. Under non-stress conditions, Nrf2 is bound to Kelch-like ECH-associated protein 1 (Keap1) in the cytoplasm. This complex directs Nrf2 polyubiquitination and degradation. During oxidative stress, Nrf2 is liberated from Keap1 and enters the nucleus, where it can form a heterodimer with the small Maf transcription factor Nrf2, to stimulate the expression of antioxidant response element (ARE)-containing genes [14]. Therefore, we investigated the possibility that Nrf2 accumulates in the nucleus after 4-HNE treatment. Cultured cardiomyocytes were treated with 4-HNE for 1 h, and nuclear extracts of these cells were subjected to immunoblotting. Nuclear accumulation of Nrf2 in response to 4-HNE treatment was observed (Fig. 4A).

To investigate whether Nrf2 signaling is important for the favorable response to 4-HNE, the cardiomyocytes were subjected to RNA interference to block Nrf2 expression and then stimulated with 4-HNE (5 μM) or vehicle for 6 h. Nrf2 silencing almost completely suppressed the 4-HNE-mediated increases in the expression levels of Gclc, xCT, and Gsta2. In contrast, Nrf2 silencing only modestly suppressed the 4-HNE-mediated increase in HO-1 expression (Fig. 4B). Therefore, we examined the possible involvement of Nrf2 in the observed increased in GSH level. Nrf2 silencing cells and control cells were treated with 4-HNE (5 μM) or vehicle for 14 h. Nrf2 silencing resulted in no appreciable cytotoxicity under these conditions (data not shown). The 4-HNE-mediated increase in GSH level was markedly suppressed in Nrf2 siRNA-treated cardiomyocytes, as compared to control siRNA-treated cardiomyocytes (115.98 ± 8.63 μM/mg vs. 213.43 ± 16.24 μM/mg, respectively) (Fig. 4C).

Next, we examined the effect of Nrf2 silencing on cardiomyocyte viabilities. Cardiomyocytes were treated with either Nrf2-specific siRNA or a control siRNA for 24 h, and then stimulated with 4-HNE (5 μM or 10 μM) for 24 h. Whereas neither 5 μM nor 10 μM 4-HNE was toxic for cardiomyocytes treated with the control siRNA (81.89% ± 2.95% for 5 μM 4-HNE; 71.97% ± 4.44% for 10 μM 4-HNE), Nrf2 silencing significantly decreased cardiomyocyte viability in the presence of 4-HNE (48.94% ± 3.30% for 5 μM 4-HNE; and 14.49% ± 1.40% for 10 μM 4-HNE) (Fig. 5A, B).

To examine the role of Nrf2 in the induction of protection mediated by 4-HNE, Nrf2-depleted cardiomyocytes were preincubated with 5 μM 4-HNE for 14 h, and then stimulated with 10 μM or 20 μM of 4-HNE for an additional 24 h. Preincubation with 5 μM 4-HNE for 14 h had no appreciable cytotoxic effect on either the Nrf2-wildtype or Nrf2-depleted cardiomyocytes. However, the viabilities of

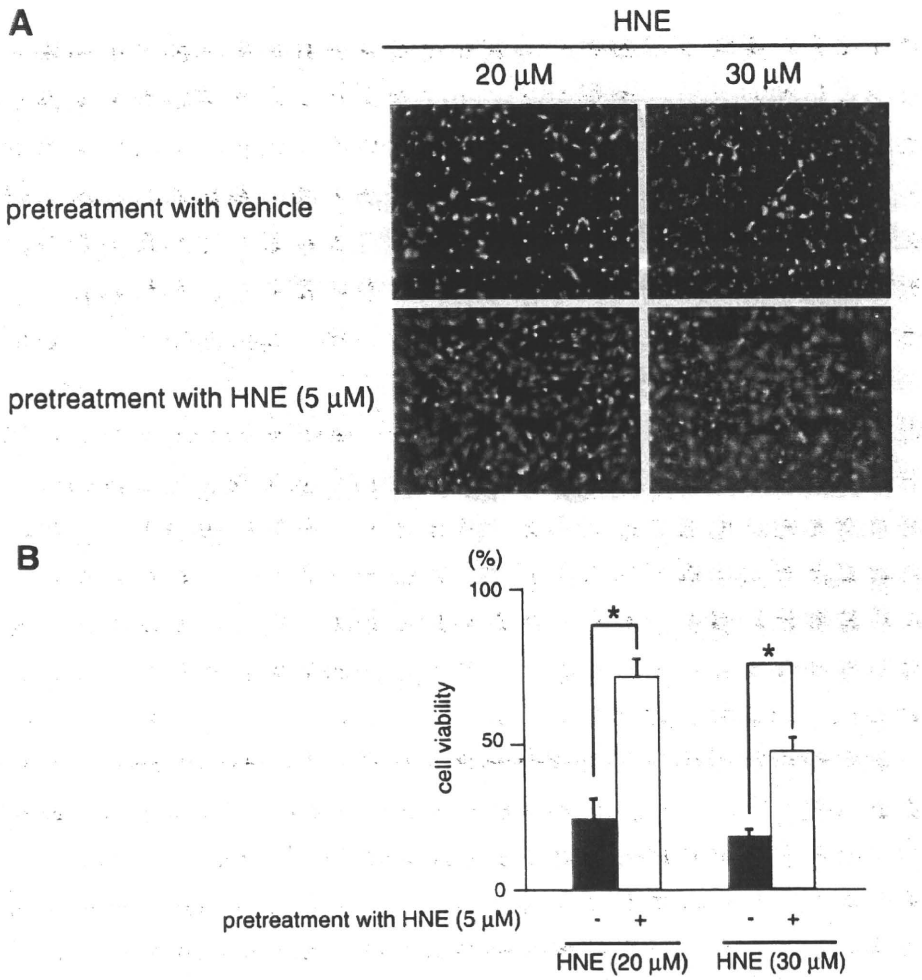

Fig. 2. Exposure to a sublethal concentration of 4-HNE enables cardiomyocytes to adapt to cytotoxic concentrations of 4-HNE. Cardiomyocytes were treated with either vehicle or 4-HNE (5 μM) for 14 h, and then incubated with a toxic concentration (20 μM or 30 μM) of 4-HNE for 24 h. (A) Representative images of cardiomyocytes that were treated with toxic concentrations of 4-HNE. (B) Quantification of cell viability. Data shown are mean ± SEM ($n = 5$). *$P<0.05$ vs. vehicle-pretreated cardiomyocytes (unpaired Student's *t*-test).

the Nrf2-depleted cardiomyocytes in 10 μM 4-HNE and 20 μM 4-HNE were 0.00% and 0.00%, respectively, while those of the control cells were 86.69% ± 3.49% and 71.18% ± 3.43%, respectively (Fig. 5C, D).

3.5. BSO treatment sensitizes cardiomyocytes to 4-HNE-induced cell death

To investigate whether GSH is an important factor in tolerance to 4-HNE, cardiomyocytes were incubated with 50 μM BSO, an inhibitor of GSH biosynthesis, in the presence or absence of 4-HNE (5 μM) for 14 h. BSO treatment decreased the intracellular GSH concentration from 162.47 ± 3.02 μM/mg (vehicle-treated cardiomyocytes) to 98.98 ± 12.13 μM/mg (BSO-treated cardiomyocytes). In addition, simultaneous 4-HNE treatment (5 μM) failed to increase the intracellular GSH levels of the BSO-treated cardiomyocytes (Fig. 6A). This concentration of BSO showed no appreciable effect on cardiomyocyte viability in the absence of 4-HNE, whereas it sensitized the cardiomyocytes to 4-HNE-induced death, as compared to the vehicle treatment. The viabilities of the vehicle-pretreated cardiomyocytes were 82.64% ± 3.07% for 5 μM 4-HNE and 72.61% ± 2.02% for 10 μM 4-HNE. Pretreatment with BSO significantly decreased the cardiomyocyte viabilities to 53.60 ± 2.79% for 5 μM 4-HNE and 35.16% ± 2.40% for 10 μM 4-HNE (Fig. 6B, C).

To examine the role of GSH biosynthesis in the induction of 4-HNE-mediated protection, cardiomyocytes were incubated with 5 μM 4-HNE in the presence of 50 μM BSO for 14 h, and then stimulated with 10 μM or 20 μM 4-HNE for an additional 24 h. The preincubation with 5 μM 4-HNE for 14 h had no appreciable cytotoxicity even in the presence of 50 μM BSO. However, the cardiomyocyte viabilities for treatment with 10 μM 4-HNE and 20 μM 4-HNE were 5.88% ± 0.46% and 0.00%, respectively, in the BSO-treated groups, and 88.52% ± 1.39% and 73.77% ± 1.60%, respectively, in the control groups (Fig. 6D, E).

3.6. 4-HNE pretreatment improves the functional recovery of Langendorff-perfused hearts after ischemia–reperfusion injury

The effect of 4-HNE treatment on function recovery after ischemia–reperfusion was studied in Langendorff-perfused mouse hearts. Mice were injected with either 4 mg/kg 4-HNE or vehicle (50 μl of saline) *via* the retro-orbital vein [12] [13], and 24 h later, the hearts were isolated and subjected to 25 min of total global ischemia, followed by 60 min of aerobic reperfusion. We selected 4 mg/kg 4-HNE as the optimal dosage based on a pilot study in which various amounts of 4-HNE were administered *via* the retro-orbital vein. We confirmed that sufficient reactive 4-HNE reaches the heart upon systemic administration within

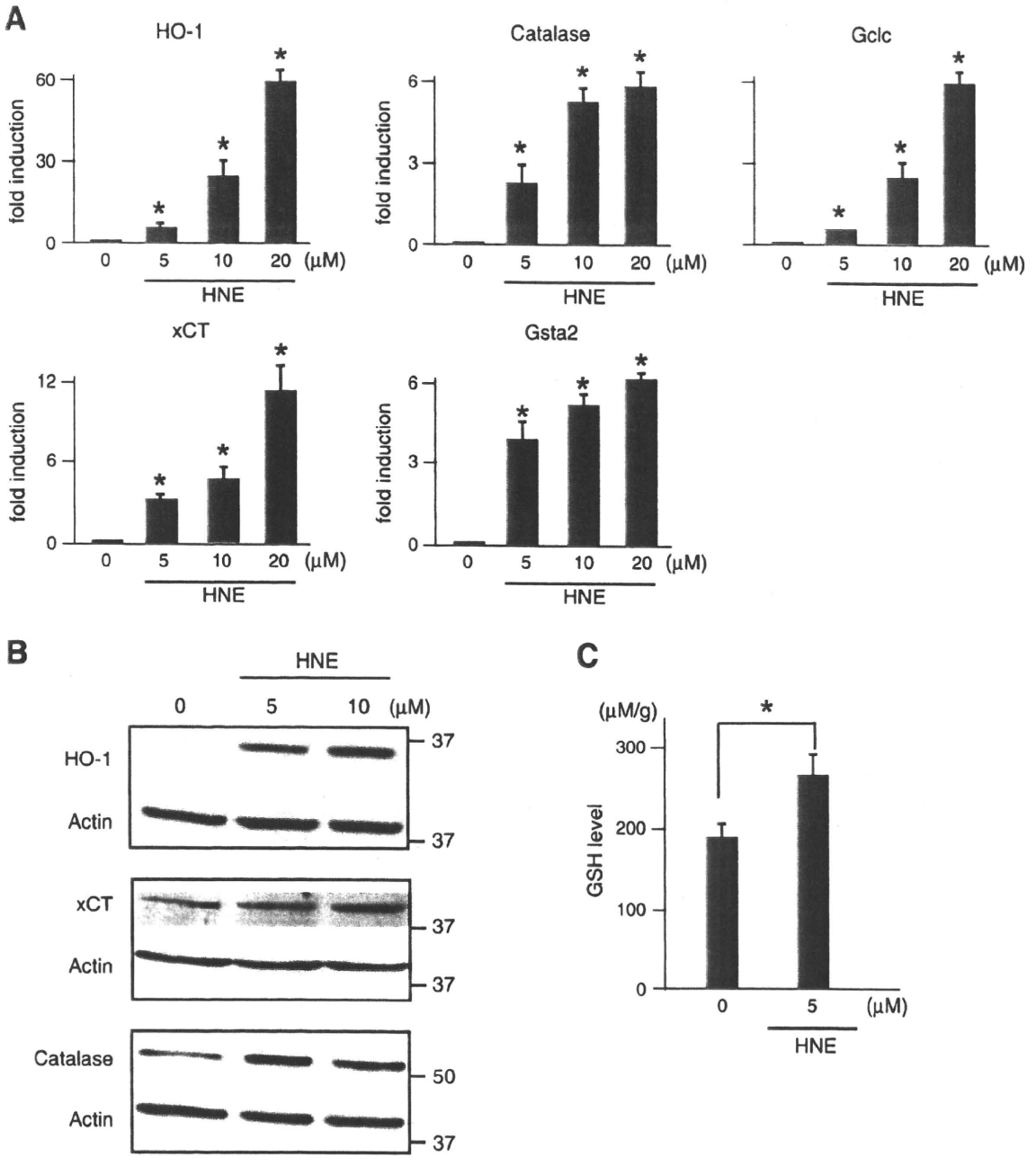

Fig. 3. 4-HNE increases the cardiomyocyte expression levels of antioxidant enzymes and GSH. (A) Cardiomyocytes were treated with different concentrations of 4-HNE (0, 5, 10, 20 μM) for 6 h. Antioxidant gene expression was determined by Q-PCR analysis. $n=5$; *$P<0.05$ vs. vehicle-treated cardiomyocytes. (B) Cardiomyocytes were treated with different concentrations of 4-HNE (0, 5, 10 μM) for 14 h. The antioxidant enzyme expression levels were determined by immunoblotting. (C) Cardiomyocytes were treated with 4-HNE for 24 h. The intracellular levels of GSH were measured using Bioxytech GSH/GSSG-412 (Oxis Research), based on the Tietze method; $n=5$, *$P<0.05$, compared to the vehicle-treated cardiomyocytes.

60 min (Supplemental Fig. 2) and activated Nrf2 in the hearts (Supplemental Fig. 3A). The administration of 4-HNE *via* the retro-orbital vein significantly upregulated the levels of mRNA for antioxidant enzymes (Supplemental Fig. 3B) and increased the GSH levels, as compared to vehicle-treated control hearts (237.41 ± 12.24 mM/g for the 4-HNE-treated group vs. 214.26 ± 4.89 mM/g for the control group; $n=4$, $P<0.05$).

4-HNE pretreatment did not affect the cardiac parameters at baseline (data not shown), whereas it significantly improved the recovery of LVDP, positive dP/dt, and negative dP/dt, as compared to the control treatment (Fig. 7). Consistent with these findings, the level of total LDH release into the perfusate during reperfusion was significantly lower in the 4-HNE-pretreatment hearts than in the control hearts.

Next, we examined the changes in the levels of 4-HNE in the hearts using antibodies specific for 4-HNE adduct proteins. Despite the significant changes in cardiac gene expression and GSH content, we did not detect any difference in the levels of 4-HNE adduct proteins between the vehicle-treated and 4-HNE-treated hearts. Ischemia–reperfusion significantly increased the levels of 4-HNE adduct proteins in the Langendorff-perfused hearts. Consistent with the significant reduction

of infarct size, pretreatment with 4-HNE significantly attenuated the increase in 4-HNE adduct proteins during reperfusion injury (Supplemental Fig. 4).

3.7. 4-HNE treatment has no effect on the functional recovery of the left ventricle after ischemia–reperfusion in Langendorff-perfused Nrf2-knockout mouse hearts

To examine the role of Nrf2 in the cardioprotective effect of 4-HNE, Nrf2-knockout mice were injected i.v. with either 4 mg/kg 4-HNE or vehicle, and 24 h later, the hearts were isolated and subjected to the same ischemia–reperfusion protocol. There was no difference in LV function before the induction of ischemia between the hearts from the Nrf2-knockout mice and those from the wild-type control mice. 4-HNE pretreatment did not affect the cardiac parameters at baseline in the Nrf2-knockout mice (data not shown). 4-HNE pretreatment did not improve the recovery of LVDP or rate-pressure product during reperfusion of the Nrf2-knockout mouse hearts. Moreover, 4-HNE pretreatment did not attenuate the total LDH activity released into the perfusate during reperfusion (Fig. 8). Notably, 4-HNE pretreatment

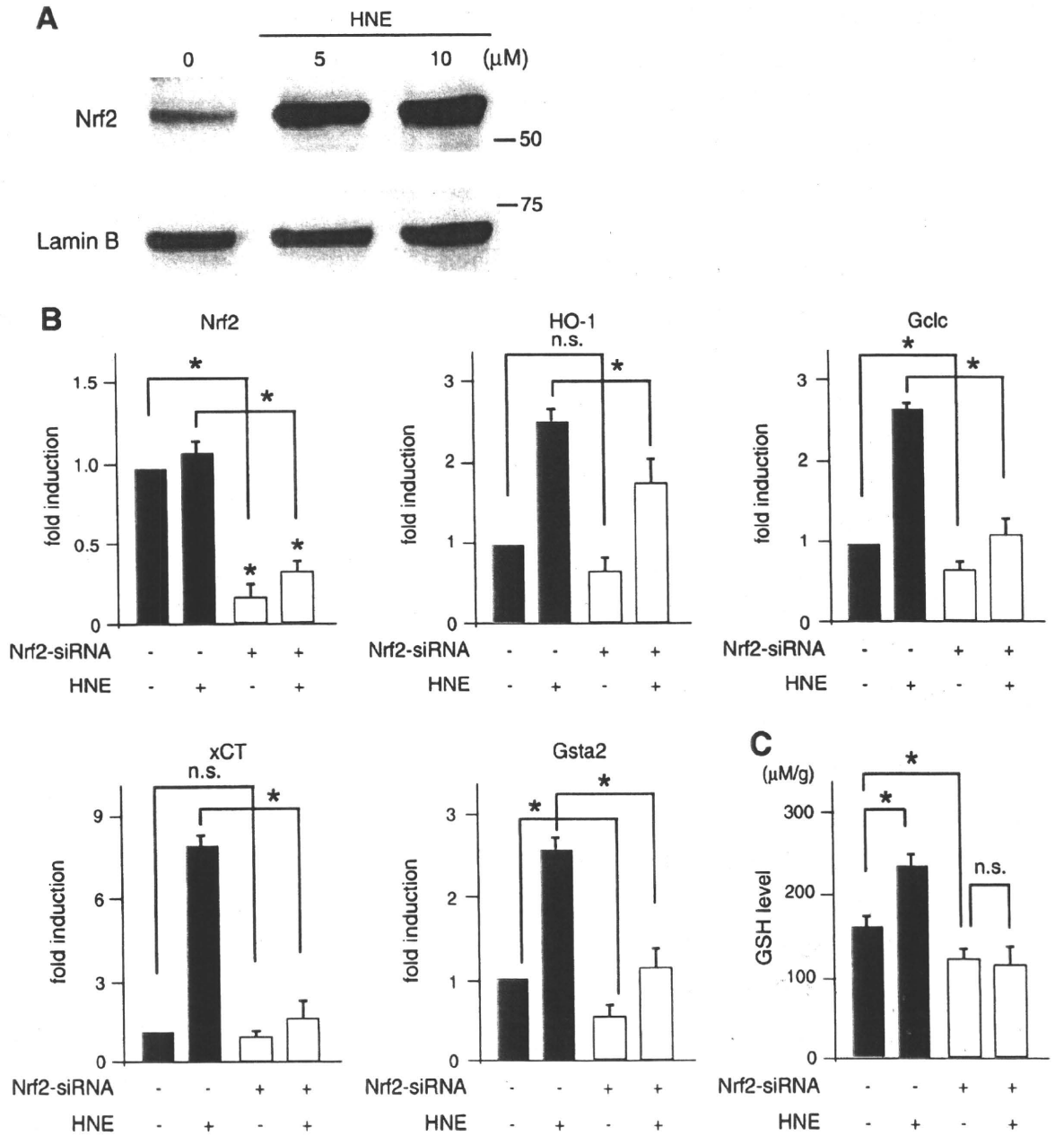

Fig. 4. Nrf2-dependent transcription is activated in 4-HNE-treated cardiomyocytes. (A) Cardiomyocytes were treated with sublethal concentrations of 4-HNE (0, 5, 10 μM) for 1 h. Nuclear extracts were subjected to SDS-PAGE, and Nrf2 was detected by immunoblotting. Membranes were stripped and reprobed with anti-Lamin B antibodies. (B) Cardiomyocytes were treated with either an Nrf2-specific siRNA or a control siRNA for 24 h, and then stimulated with 4-HNE (5 μM) for 6 h. Antioxidant gene expression was determined by Q-PCR analysis; $n=5$, $^*P<0.05$, compared to control siRNA-treated cardiomyocytes. (C) The intracellular levels of GSH were measured 14 h after 4-HNE (5 μM) treatment using Bioxytech GSH/GSSG-412 (Oxis Research), based on the Tietze method; $n=5$, $^*P<0.05$, compared to control siRNA-treated cardiomyocytes without 4-HNE stimulation.

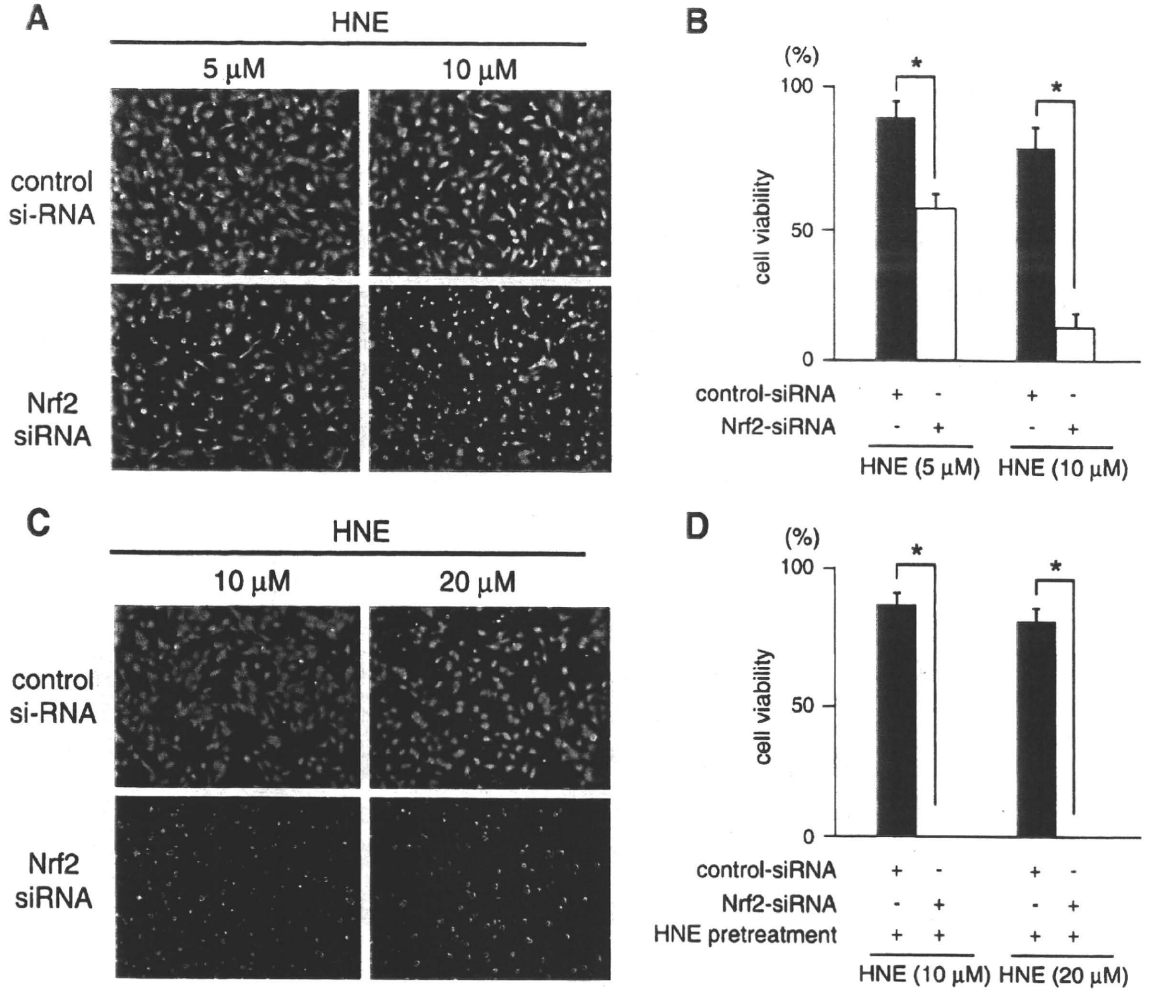

Fig. 5. Nrf2-deficient cardiomyocytes exhibit lower resistance to oxidative stress and the adaptive response to 4-HNE is completely abolished. Cardiomyocytes were treated with either Nrf2-specific siRNA or a control siRNA for 24 h, and then stimulated with 4-HNE (5 μM or 10 μM) for 24 h. (A) Representative images of cardiomyocytes after treatment with different concentrations of 4-HNE. (B) Quantification of cell viability. Data shown are mean ± SEM ($n = 5$). *$P<0.05$ vs. control siRNA-treated cardiomyocytes (unpaired Student's t-test). Nrf2-depleted cardiomyocytes were preincubated with 5 μM 4-HNE for 14 h, and then stimulated with 4-HNE (10 μM or 20 μM) for 24 h. (C) Representative images of cardiomyocytes after treatment with different concentrations of 4-HNE. (D) Quantification of cell viability. Data shown are mean ± SEM ($n = 5$). *$P<0.05$ vs. control siRNA-treated cardiomyocytes (unpaired Student's t-test).

increased the protein expression levels of xCT, GPX4, Gclc, Gsta, HO-1, and Catalase in the Nrf-2 wild-type hearts, but not in the Nrf2-knockout hearts (Supplemental Fig. 5).

4. Discussion

In addition to the pathogenic effects associated with oxidative stress, 4-HNE is considered to play an important role as a signal transduction molecule in stimulating the antioxidant defense network. This induction of stress-protective mechanisms is referred to as "stress-response hormesis" [9]. The present study provides insights into the clinical significance of stress-response hormesis induced by 4-HNE (Supplemental Fig. 7).

Hormesis is generally defined as a biphasic dose–response curve to a treatment that is beneficial at low levels but noxious at higher levels [15]. However, for practical reasons, most researchers in the fields of aging and molecular biology use a limited number of dosages within the optimal or hormetic zone when studying adaptive mechanisms. Thus, these researchers report hormetic effects without having to confirm the biphasic dose–response curve. This is certainly true for many examples of preconditioning. In the present study, we show a biphasic dose–response curve; 4-HNE induced cardiomyocyte death at higher concentrations (≥20 μM), whereas it had no appreciable cytotoxicity at lower concentrations (≤10 μM). Notably, a lower concentration of 4-HNE primed the cardiomyocytes for subsequent oxidative injury, thereby enabling the cells to adapt to cytotoxic concentrations of 4-HNE. Furthermore, we demonstrate that the administration of 4-HNE *via* the retro-orbital vein protects the heart against cell death induced by ischemia–reperfusion injury. 4-HNE pretreatment significantly attenuated the accumulation of 4-HNE adduct proteins during reperfusion. A growing body of evidence indicates that a brief ischemic insult in one organ releases endogenous factors that protect other organs against a prolonged ischemic insult [16]. This phenomenon is known as 'remote ischemic preconditioning'. The exact nature of signaling transduction from remote tissue to target organ remains to be fully elucidated. Aldehydes are more stable than their precursor ROS, which means that they can diffuse to sites at a distance from their site of injury. Aldehydes conjugate with receptive nucleophiles, such as glutathione. In the present study, we raise the possibility that aldehydes and/or their metabolites act as humoral mediators to mediate distant organ protection.

We show that Nrf2 is a key transcriptional regulator for 4-HNE-mediated establishment of antioxidative defenses, at least under acute conditions. These results are consistent with recent reports that

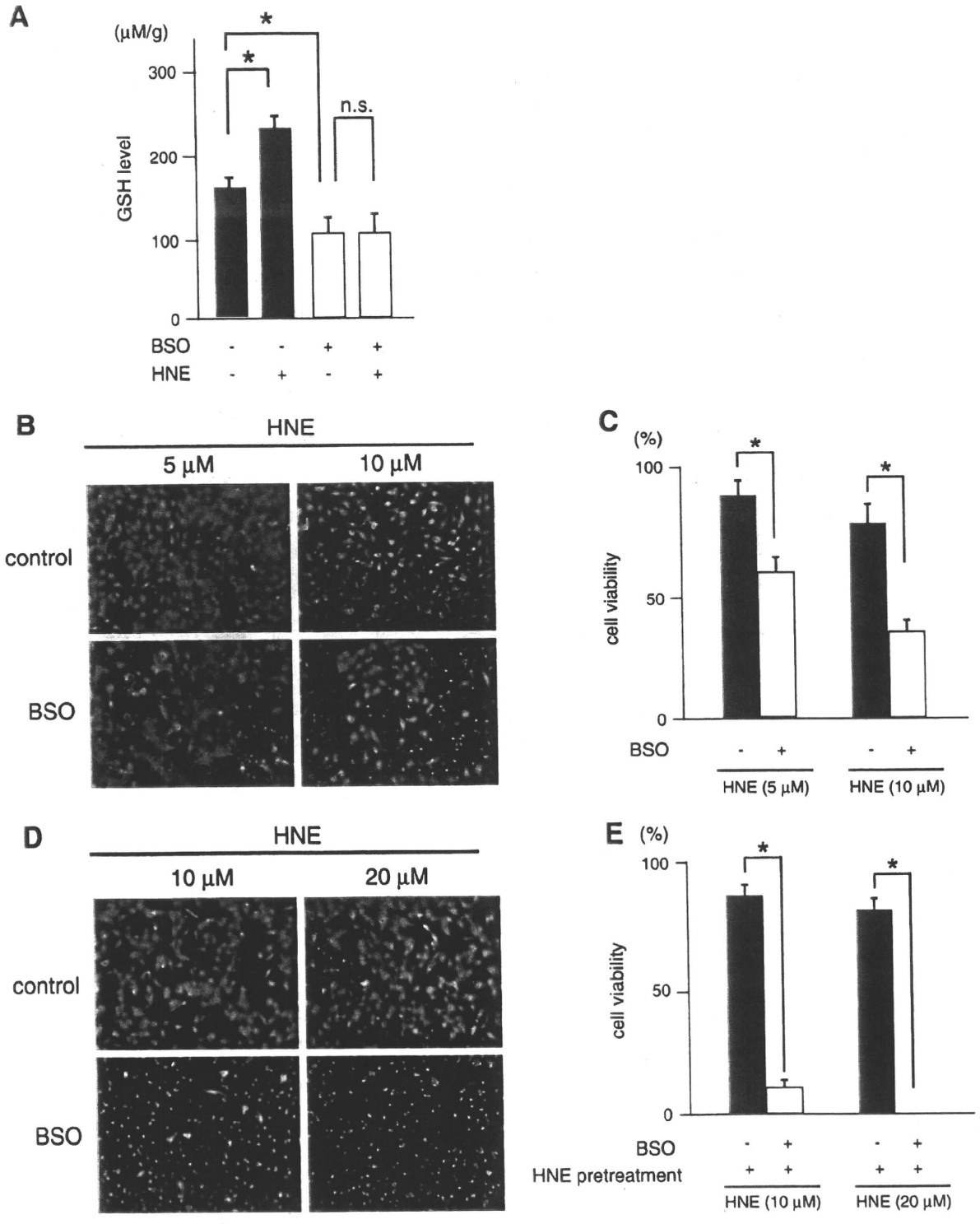

Fig. 6. Depletion of intracellular GSH using BSO renders cardiomyocytes less tolerant to 4-HNE and abolishes the 4-HNE-induced preconditioning effect. (A) Cardiomyocytes were incubated with 50 μM BSO in the presence or absence of 4-HNE (5 μM) for 14 h. The intracellular levels of GSH were measured using Bioxytech GSH/GSSG-412 (Oxis Research), based on the Tietze method; $n = 5$, $^*P<0.05$, compared to BSO-untreated cardiomyocytes without 4-HNE stimulation. (B) Cardiomyocytes were incubated with 50 μM BSO, and then stimulated with 4-HNE for 24 h. Representative images of cardiomyocytes after treatment with 4-HNE. (C) Quantification of cell viability. Data shown are mean ± SEM ($n = 5$). $^*P<0.05$ vs. BSO-untreated cardiomyocytes. (D) Cardiomyocytes were preconditioned with 4-HNE (5 μM) in the presence or absence of 50 μM BSO for 14 h, and then examined for tolerance to higher dosages (10 μM and 20 μM) of 4-HNE. Representative images of cardiomyocytes after treatment with 4-HNE. (E) Quantification of cell viability. Data shown are mean ± SEM ($n = 5$). $^*P<0.05$ vs. 4-HNE-preconditioned cardiomyocytes without BSO treatment.

Nrf2 signaling plays an important role in 3H-1,2-dithiole-3-thione (D3T)- or H_2O_2-induced protection against oxidative injury to cardiomyocytes [17] [18]. Under unstressed conditions, Nrf2 is tethered to Keap1 in the cytoplasm. This complex directs Nrf2 polyubiquitination and degradation. During oxidative stress, Nrf2 is liberated from Keap1 and enters the nucleus, where it forms a

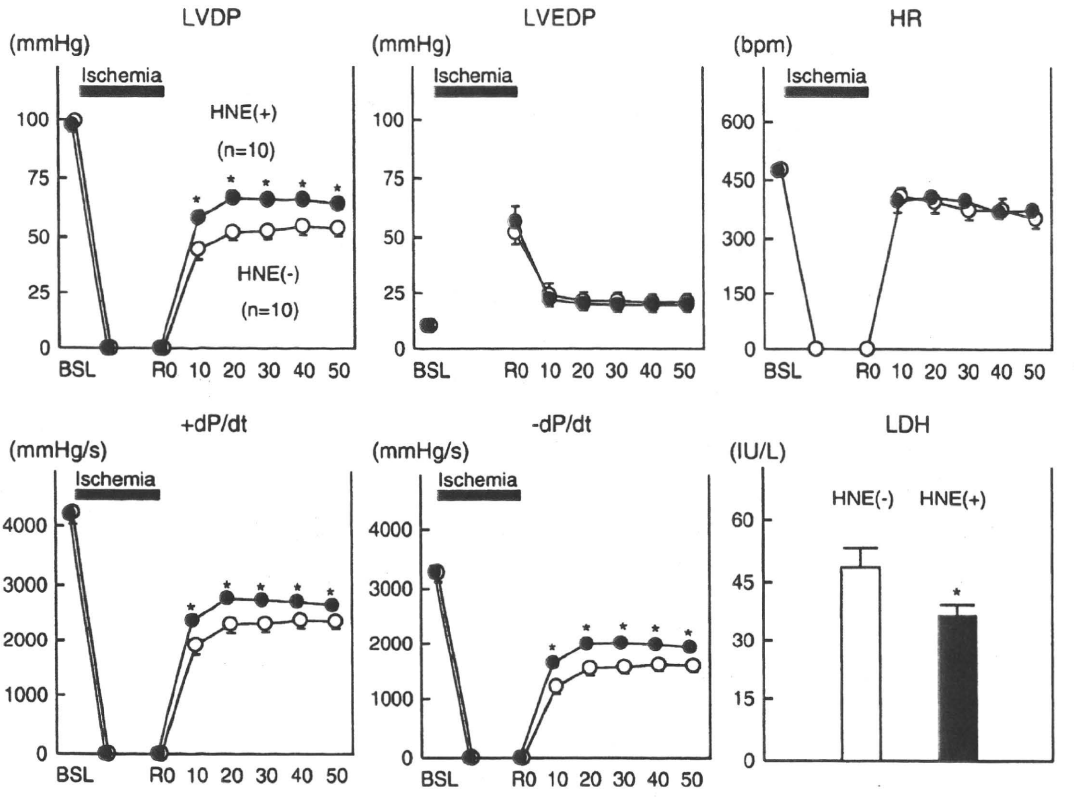

Fig. 7. 4-HNE treatment significantly improves the functional recovery of the left ventricle after ischemia–reperfusion in Langendorff-perfused hearts. The stock solution of 4-HNE was diluted with PBS, and a dose of 4 mg/kg HNE was administered via the retro-orbital vein 24 hours before sacrifice under anesthesia using diethyl ether. A vehicle solution (ethanol diluted with PBS) was administered in the same manner. Twenty-four hours later, the hearts were excised rapidly under deep anesthesia using pentobarbital and were immediately mounted on the Langendorff apparatus. Langendorff-perfused hearts were subjected to 25 min of total global ischemia, followed by aerobic reperfusion. LVDP, Recovery of left ventricular developing pressure; LVEDP, diastolic pressure; HR, heart rate; $+/-dP/dt$, peak positive/negative dP/dt; RPP, rate pressure product. $^*P<0.05$ for HNE-preconditioned hearts ($n=10$) vs. control hearts ($n=10$) (unpaired Student's t-test).

heterodimer with the small Maf transcription factor Nrf2, to induce the expression of genes for proteins that function as antioxidants and enzymes that are involved in phase II detoxification and glutathione biosynthesis [14]. The mechanism by which 4-HNE induces the nuclear accumulation of Nrf2 remains to be clarified. Specific cysteine residues (Cys273/Cys288) in the Keap1 protein are known to act as a sensor for oxidative stress, and modification of these residues leads to a conformational change in Keap1, with consequent release of Nrf2 [19]. 4-HNE induces a conformational change in Keap1 directly *via* adduct formation or indirectly by increasing the production of mitochondrial ROS [20].

There is accumulating evidence that the myocardial GSH content influences susceptibility to ischemia–reperfusion injury [21]. N-acetylcysteine and γ-glutamyl-cysteine ethyl ester, which are precursors in glutathione biosynthesis, significantly attenuate myocardial ischemia–reperfusion injury when administered before reperfusion [22]. In contrast, glutathione depletion exacerbates myocardial ischemia–reperfusion injury [21,23]. We show that the stimulation of cellular GSH biosynthesis through the up-regulation of GCL, a rate-limiting enzyme in GSH biosynthesis, plays a crucial role in 4-HNE-mediated cardioprotection *via* Nrf2 activation. Reduction of the GSH content to about 100 μM/g by either Nrf2-siRNA or BSO (a GCL inhibitor) sensitized the cardiomyocytes to 4-HNE-induced death and completely abolished the cardioprotective effect of a low dose of 4-HNE.

In addition to Nrf2, activating transcription factor 4 (ATF4) is also activated following the induction of oxidative stress and GSH biosynthesis [24]. Recently, we reported that life-long mitochondrial oxidative stress increases the phosphorylation levels of the α-subunit of translation initiation factor 2 (eIF2α) [25]. Phosphorylation of eIF2α inhibits general protein synthesis, although it specifically stimulates the translation of ATF4. ATF4 stimulates the expression of genes that encode enzymes that are involved in serine biosynthesis, while it does not stimulate the expression of GCL. Serine is a precursor of glycine and cysteine, both of which are needed for the biosynthesis of GSH. ATF4 also stimulates the expression of the solute-like carrier family of amino acid transporters. Thus, ATF4 activates GSH biosynthesis by providing the amino acids necessary for glutathione biosynthesis.

The rate of GSH synthesis is determined primarily by GCL activity and the availability of precursor amino acids. In the acute setting, Nrf-2-dependent induction of GCL expression mainly contributes to the enhanced production of GSH, thereby replenishing the intracellular GSH pool. However, once the intracellular GSH is recovered to normal levels, GCL activity is subject to feedback inhibition by GSH. To maintain in the long-term the increased levels of GSH so as to re-establish homeostasis under persistent oxidative stress, cardiomyocytes shift their glucose metabolism from mitochondrial oxidative energy production to the generation of reducing equivalents (NADPH or GSH) in the cytosol by activating the pentose phosphate pathway and amino acid metabolism *via* an ATF4-dependent mechanism [25]. Thus, Nrf2 and ATF4 appear to act in a co-ordinated manner to regulate glutathione biosynthesis and the glutathione redox cycle at different time-points [26].

Although the baseline expression levels of catalase, Gclc, and Gsta were suppressed by up to 50% in the Nrf2-knockout hearts, as compared to the wild-type hearts (Zhang and Sano, unpublished observation), the Nrf2-knockout hearts were phenotypically normal under the unstressed condition. However, the preconditioning effect of 4-HNE was

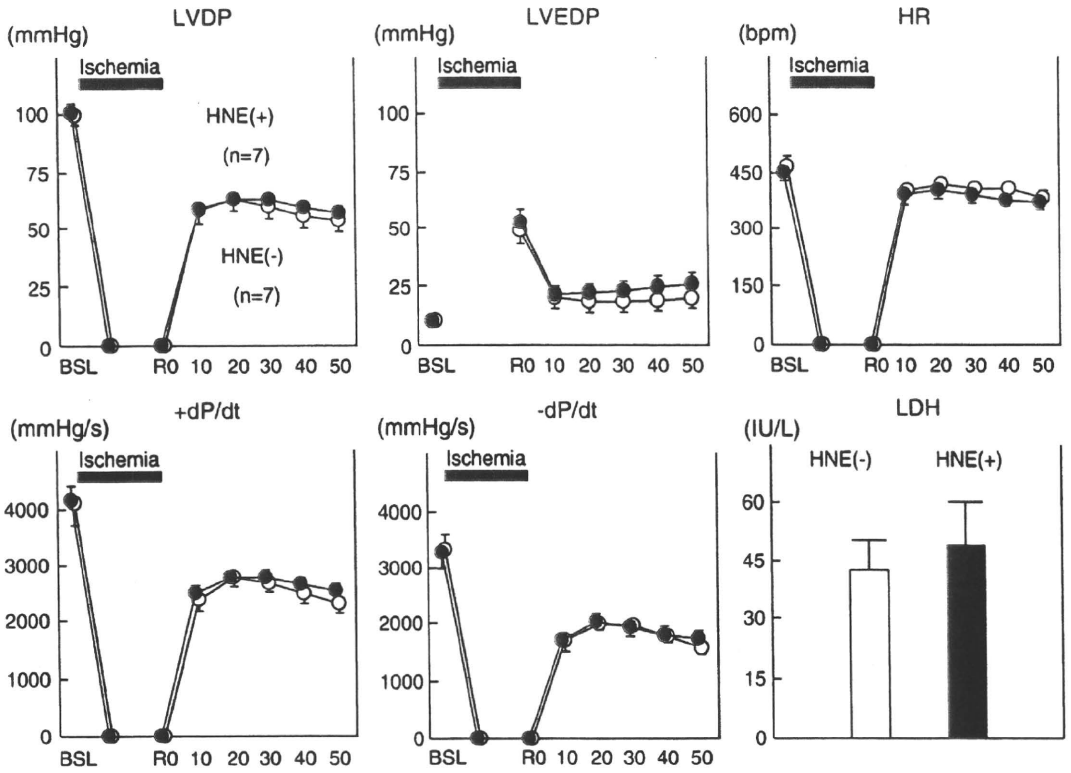

Fig. 8. 4-HNE treatment has no effect on the functional recovery of the left ventricle after ischemia–reperfusion in Langendorff-perfused Nrf2-knockout mouse hearts. 4-HNE (4 mg/kg) was injected into the ocular vein of each mouse. Langendorff-perfused hearts were subjected to 25 min of total global ischemia, followed by aerobic reperfusion. LVDP, Recovery of left ventricular developing pressure; LVEDP, diastolic pressure; HR, heart rate; $+/-dP/dt$, peak positive/negative dP/dt; RPP, rate pressure product. $^{*}P<0.05$ for HNE-preconditioned ($n=7$) vs. control hearts ($n=7$) (unpaired Student's t-test).

completely absent in the Nrf2-knockout hearts. These results indicate that either Nrf2 is dispensable or that the Nrf2 defect is completely compensated for under the unstressed condition but is indispensable for the acute adaptive response under conditions of stress. Consistent with this notion, Nrf2-knockout hearts are prone to progression to terminal heart failure in response to pressure-overload by TAC [27]. Interestingly, the recovery of positive and negative dP/dt during early reperfusion was better in the Nrf2-knockout hearts than in the Nrf2-wildtype hearts (20 min of reperfusion and 10, 20, and 30 min of reperfusion, respectively) (Supplemental Fig. 4). The recovery of LVDP during early reperfusion tended to be better in Nrf2-KO mice, although the difference between Nrf2-wild-type and Nrf2-knockout mice was not statistically significant. These results strongly suggest that a compensatory mechanism against oxidative stress is stimulated in Nrf2-KO mice. However, the cardioprotection observed in the Nrf2-knockout mice was transient, and the recovery of LV function was similar in the two groups during late reperfusion (Supplemental Fig. 6). In addition, the finding that there was no difference in the total LDH activity released into the perfusate during reperfusion indicates that the extent of irreversible damage after ischemia–reperfusion is equivalent in Nrf2-wild-type and Nrf2-knockout mice, at least in these Langendorff-perfused hearts. 4-HNE pretreatment significantly improved the recovery of LV function during overall reperfusion, and attenuated LDH release during reperfusion in Nrf2-wildtype mice. Cardiac Nrf-2 was activated in the heart 60 min after the injection of 4-HNE via the retro-orbital vein. Both the up-regulation of cardiac anti-oxidant enzymes and the cardioprotection afforded by 4-HNE pretreatment were completely abrogated in the Nrf2- knockout mice. Therefore, we conclude that Nrf2 is essential for 4-HNE-induced cardioprotection, despite the differences in the patterns of LV functional recovery observed between Nrf2-wildtype and Nrf2-knockout mice. The mechanism by which Nrf2- knockout mice manifest improved LV function during early reperfusion remains unknown.

4-HNE is highly reactive so that most of 4-HNE may undergo nucleophilic addition reactions with electron-rich centers particularly non-protein and protein thiols and amines in the blood. Thus, we examined whether sufficient reactive 4-HNE reaches the heart upon systemic administration using antibodies specific for 4-HNE adduct proteins and showed that the level of 4-HNE in the heart was increased at 60 min after the administration of 4-HNE via the retro-orbital vein. We also demonstrated that cardiac Nrf2 is activated at 60 min after systemic administration of 4-HNE. We concluded that 4-HNE or 4-HNE conjugate metabolite can reaches the heart upon systemic administration and stimulate intracellular signaling in the heart. Notably, not only free 4-HNE but also 4-HNE conjugate metabolite can stimulate intracellular signaling and increased cell growth in cultured vascular smooth muscle cells [28].

Several studies have suggested that the generation of aldehydes, such as 4-HNE, contributes to much of the damage induced by ROS [29]. The present study intriguingly shows that a sublethal concentration of 4-HNE protects cardiomyocytes from ischemia–reperfusion injury. An improved understanding of the dual roles of 4-HNE would facilitate the design of novel strategies for cardioprotection against oxidative stress [30].

Disclosures

None.

Sources of funding

This work was supported by the Japan-China Medical Association (to Y.Z.) and by a PRESTO (Metabolism and Cellular Function) grant from the Japanese Science and Technology Agency (to M.S.).

Acknowledgments

The authors thank the Japan-China Medical Association and the Japan Foundation for giving Y. Zhang the opportunity to join our laboratory. The authors thank Y. Miyake, H. Shiozawa, M. Abe, and M. Doi for technical assistance. M. Sano and M. Suematsu are core members of the Global Center of Excellence (GCOE) for Human Metabolomics Systems Biology at MEXT.

Appendix A. Supplementary data

Supplementary data associated with this article can be found, in the online version, at doi:10.1016/j.yjmcc.2010.05.011.

References

[1] Conklin D, Prough R, Bhatanagar A. Aldehyde metabolism in the cardiovascular system. Mol Biosyst 2007 Feb;3(2):136–50.
[2] Watson AD, Leitinger N, Navab M, Faull KF, Horkko S, Witztum JL, et al. Structural identification by mass spectrometry of oxidized phospholipids in minimally oxidized low density lipoprotein that induce monocyte/endothelial interactions and evidence for their presence in vivo. J Biol Chem 1997 May 23;272 (21):13597–607.
[3] Liu Q, Raina AK, Smith MA, Sayre LM, Perry G. Hydroxynonenal, toxic carbonyls, and Alzheimer disease. Mol Aspects Med Aug-Oct 2003;24(4-5):305–13.
[4] Chen CH, Budas GR, Churchill EN, Disatnik MH, Hurley TD, Mochly-Rosen D. Activation of aldehyde dehydrogenase-2 reduces ischemic damage to the heart. Science 2008 Sep 12;321(5895):1493–5.
[5] Honarbakhsh S, Schachter M. Vitamins and cardiovascular disease. Br J Nutr 2009 Apr;101(8):1113–31.
[6] Uchida K, Shiraishi M, Naito Y, Torii Y, Nakamura Y, Osawa T. Activation of stress signaling pathways by the end product of lipid peroxidation. 4-hydroxy-2-nonenal is a potential inducer of intracellular peroxide production. J Biol Chem 1999 Jan 22;274(4):2234–42.
[7] Dickinson DA, Iles KE, Watanabe N, Iwamoto T, Zhang H, Krzywanski DM, et al. 4-hydroxynonenal induces glutamate cysteine ligase through JNK in HBE1 cells. Free Radic Biol Med 2002 Oct 1;33(7):974.
[8] Chen ZH, Saito Y, Yoshida Y, Sekine A, Noguchi N, Niki E. 4-Hydroxynonenal induces adaptive response and enhances PC12 cell tolerance primarily through induction of thioredoxin reductase 1 via activation of Nrf2. J Biol Chem 2005 Dec 23;280(51):41921–7.
[9] Gems D, Partridge L. Stress-response hormesis and aging: "that which does not kill us makes us stronger". Cell Metab 2008 Mar;7(3):200–3.
[10] Iida K, Itoh K, Kumagai Y, Oyasu R, Hattori K, Kawai K, et al. Nrf2 is essential for the chemopreventive efficacy of oltipraz against urinary bladder carcinogenesis. Cancer Res 2004 Sep 15;64(18):6424–31.
[11] Tokudome S, Sano M, Shinmura K, Matsuhashi T, Morizane S, Moriyama H, et al. Glucocorticoid protects rodent hearts from ischemia/reperfusion injury by activating lipocalin-type prostaglandin D synthase-derived PGD2 biosynthesis. J Clin Invest 2009 Jun;119(6):1477–88.
[12] Hyafil F, Vergely C, Du Vignaud P, Grand-Perret T. In vitro and in vivo reversal of multidrug resistance by GF120918, an acridonecarboxamide derivative. Cancer Res 1993 Oct 1;53(19):4595–602.
[13] Kettner A, Kumar L, Anton IM, Sasahara Y, de la Fuente M, Pivniouk VI, et al. WIP regulates signaling via the high affinity receptor for immunoglobulin E in mast cells. J Exp Med 2004 Feb 2;199(3):357–68.
[14] Motohashi H, Yamamoto M. Nrf2-Keap1 defines a physiologically important stress response mechanism. Trends Mol Med 2004 Nov;10(11):549–57.
[15] Calabrese EJ, Baldwin LA, Holland CD. Hormesis: a highly generalizable and reproducible phenomenon with important implications for risk assessment. Risk Anal 1999 Apr;19(2):261–81.
[16] Kharbanda RK, Nielsen TT, Redington AN. Translation of remote ischaemic preconditioning into clinical practice. Lancet 2009 Oct 31;374(9700):1557–65.
[17] Zhu H, Jia Z, Misra BR, Zhang L, Cao Z, Yamamoto M, et al. Nuclear factor E2-related factor 2-dependent myocardiac cytoprotection against oxidative and electrophilic stress. Cardiovasc Toxicol Summer 2008;8(2):71–85.
[18] Purdom-Dickinson SE, Lin Y, Dedek M, Morrissy S, Johnson J, Chen QM. Induction of antioxidant and detoxification response by oxidants in cardiomyocytes: evidence from gene expression profiling and activation of Nrf2 transcription factor. J Mol Cell Cardiol 2007 Jan;42(1):159–76.
[19] Kobayashi A, Kang MI, Watai Y, Tong KI, Shibata T, Uchida K, et al. Oxidative and electrophilic stresses activate Nrf2 through inhibition of ubiquitination activity of Keap1. Mol Cell Biol 2006 Jan;26(1):221–9.
[20] Hill BG, Dranka BP, Zou L, Chatham JC, Darley-Usmar VM. Importance of the bioenergetic reserve capacity in response to cardiomyocyte stress induced by 4-hydroxynonenal. Biochem J 2009 Nov 15;424(1):99–107.
[21] Singh A, Lee KJ, Lee CY, Goldfarb RD, Tsan MF. Relation between myocardial glutathione content and extent of ischemia–reperfusion injury. Circulation 1989 Dec;80(6):1795–804.
[22] Hoshida S, Kuzuya T, Yamashita N, Nishida M, Kitahara S, Hori M, et al. gamma-Glutamylcysteine ethyl ester for myocardial protection in dogs during ischemia and reperfusion. J Am Coll Cardiol 1994 Nov 1;24(5):1391–7.
[23] Blaustein A, Deneke SM, Stolz RI, Baxter D, Healey N, Fanburg BL. Myocardial glutathione depletion impairs recovery after short periods of ischemia. Circulation 1989 Nov;80(5):1449–57.
[24] Harding HP, Zhang Y, Zeng H, Novoa I, Lu PD, Calfon M, et al. An integrated stress response regulates amino acid metabolism and resistance to oxidative stress. Mol Cell 2003 Mar;11(3):619–33.
[25] Endo J, Sano M, Katayama T, Hishiki T, Shinmura K, Morizane S, et al. Metabolic remodeling induced by mitochondrial aldehyde stress stimulates tolerance to oxidative stress in the heart. Circ Res 2009 Nov 20;105(11):1118–27.
[26] Sano M, Fukuda K. Activation of mitochondrial biogenesis by hormesis. Circ Res 2008 Nov 21;103(11):1191–3.
[27] Li J, Ichikawa T, Villacorta L, Janicki JS, Brower GL, Yamamoto M, et al. Nrf2 protects against maladaptive cardiac responses to hemodynamic stress. Arterioscler Thromb Vasc Biol Jul 10 2009.
[28] Ramana KV, Bhatnagar A, Srivastava S, Yadav UC, Awasthi S, Awasthi YC, et al. Mitogenic responses of vascular smooth muscle cells to lipid peroxidation-derived aldehyde 4-hydroxy-trans-2-nonenal (HNE): role of aldose reductase-catalyzed reduction of the HNE-glutathione conjugates in regulating cell growth. J Biol Chem 2006 Jun 30;281(26):17652–60.
[29] Veronneau M, Comte B, Des Rosiers C. Quantitative gas chromatographic-mass spectrometric assay of 4-hydroxynonenal bound to thiol proteins in ischemic/reperfused rat hearts. Free Radic Biol Med 2002 Nov 15;33(10):1380–8.
[30] Hill BG, Bhatnagar A. Beyond reactive oxygen species: aldehydes as arbitrators of alarm and adaptation. Circ Res 2009 Nov 20;105(11):1044–6.

Autonomic Neuroscience: Basic and Clinical 156 (2010) 27–35

Contents lists available at ScienceDirect

Autonomic Neuroscience: Basic and Clinical

journal homepage: www.elsevier.com/locate/autneu

Norepinephrine-induced nerve growth factor depletion causes cardiac sympathetic denervation in severe heart failure

Kensuke Kimura *, Hideaki Kanazawa, Masaki Ieda, Haruko Kawaguchi-Manabe, Yoshiko Miyake, Takashi Yagi, Takahide Arai, Motoaki Sano, Keiichi Fukuda

Department of Regenerative Medicine and Advanced Cardiac Therapeutics, Keio University School of Medicine, 35 Shinanomachi, Shinjuku-ku, Tokyo 160-8582, Japan

ARTICLE INFO

Article history:
Received 6 November 2009
Received in revised form 25 February 2010
Accepted 26 February 2010

Keywords:
Sympathetic denervation
Congestive heart failure
Nerve growth factor
Norepinephrine

ABSTRACT

In severe congestive heart failure (CHF), sympathetic overactivity correlates with the exacerbation of cardiac performance. To test the hypothesis that the cardiac sympathetic nerve density dramatically changes with the acceleration of circulating norepinephrine (NE) concentration, we investigated the temporal association of nerve growth factor (NGF) expression in the heart and cardiac sympathetic nerve density during the development of CHF in the continuous NE-infused rats. The animals were analyzed at 0-, 1-, 3-, 7-, 14-, and 28-day after implantation of osmotic pump at a rate of 0.05 mg/kg/hr. The cardiac performance was temporally facilitated in NE-exposed rats at 3-day in accordance with the sympathetic hyper-innervation induced by the augmentation of NGF mRNA expression in the heart. In NE-treated rats, left ventricular end-diastolic pressure was significantly increased after 7-day and marked left ventricular hypertrophy and systemic fluid retention were observed at 28-day. CHF-induced sympathetic overactivity further increased plasma NE concentration in NE-treated rats and finally reached to 16.1 ± 5.6 ng/ml at 28-day (control level was 0.39 ± 0.1 ng/ml, $p<0.01$). In the decompensated CHF rats at 28-day, the NGF mRNA expression was conspicuously reduced concomitant with the obvious nerve fiber loss confirmed by the immunostaining of nerve axonal marker, PGP9.5 and sympathetic neuron marker, tyrosine hydroxylase. This resulted in the attenuated tissue NE contents and the exacerbating cardiac performance. The cardiac sympathetic fiber loss was also confirmed in NE-exposed DBH (dopamine β-hydroxylase)-Cre/Floxed-EGFP (enhanced green fluorescent protein) mice with severe CHF, in which sympathetic nerve could be traced by EGFP. Our results suggest that the cardiac sympathetic nerve density is strictly regulated by the NGF expression in the heart and long-exposure of high plasma NE concentration caused myocardial NGF reduction, following sympathetic fiber loss in severe CHF animals.

1. Introduction

It is well known that plasma norepinephrine (NE) concentration is high in the patients with congestive heart failure (CHF) due to the extreme activation of sympathetic nervous system (SNS), which is progressively augmented corresponding to the severity of CHF (Thomas and Marks, 1978). Moreover, the activation of the cardiac SNS in CHF correlates with the adverse outcome (Cohn et al., 1984). Recent clinical studies have shown that the administration of β-adrenergic receptor blockers improve cardiac performance and reduce cardiac mortality (Packer et al., 1996). NE spillover from sympathetic neurons and the impaired neuronal reuptake have been considered as the major causes of the high plasma concentration in CHF (Hasking et al., 1986; Himura et al., 1993). However, the reduced gene expression of NE synthetic enzyme and NE transporter in the innervated nerves resulting depletion of NE in the failing myocardium cast doubt whether the cardiac sympathetic neurons are still activating in severe CHF (Pool et al., 1967; Eisenhofer et al., 1996). Although the existence of the cardiac-innervated sympathetic neurons which are responsible for synthesizing and secreting NE seems to be of little significance under the circumstance of highly augmented plasma NE level, the innervation anatomy and the source of increased NE overflow remains unexplained so far.

Nerve growth factor (NGF) is a prototypic member of the neurotrophin family, which is critical for the differentiation, maturation, survival, and synaptic activity of the peripheral sympathetic and sensory nervous sytem (Snider, 1994). Expression levels of NGF within innervated tissues roughly correspond to innervations density (Heumann et al., 1984). Some recent studies focused on the decreased myocardial NGF expression in CHF, however the direct evidence of the anatomically "denervated" sympathetic fibers lacked in severe heart failure (Kaye et al., 2000; Qin et al., 2002). We recently reported that the augmentation of NGF expression causes cardiac sympathetic hyperinnervation in the compensated cardiac hypertrophy (Kimura et al., 2007).

* Corresponding author. Tel.: +81 353633874; fax: +81 353633875.
E-mail address: kimuken@cpnet.med.keio.ac.jp (K. Kimura).

1566-0702/$ – see front matter © 2010 Elsevier B.V. All rights reserved.
doi:10.1016/j.autneu.2010.02.005

Given the previous clinical and experimental evidence, we hypothesized that the cardiac sympathetic nerve density dramatically changes with the acceleration of circulating NE concentration and subsequently affects the cardiac performance. To test this hypothesis in vivo, we carried out the present study to examine the temporal association of NGF expression in the heart and cardiac sympathetic nerve density during the development of CHF in the continuous NE-infused rats.

2. Materials and Methods

2.1. Animal experiments

Seven-week old male Wistar rats weighting 240 to 260 g (CLEA Japan,Inc.) were divided into two experimental groups; (1) vehicle-infusion as control groups and (2) NE-infused rats. 0.9% saline with ascorbate (1 mmol/L) vehicle or (-)norepinephrine bitartrate (Sigma Chemical Co.) dissolved in 0.9% saline with ascorbate (1 mmol/L) was administered continuously by subcutaneously implanted osmotic mini pumps (ALZET Osmotic Pumps, model 2004) into the interscapular region. Rats were sedated with ketamine (60 mg/kg) and xylasine (15 mg/kg) given intraperitoneally. NE was infused at a rate of 0.05 mg/kg/hr for maximum 28 days. The animals were killed at 0-, 1-, 3-, 7-, 14-, and 28-day after implantation of osmotic pumps. On the day of the experiment, rats were artificially ventilated under anesthesia with ketamine (60 mg/kg) and xylasine (60 mg/kg) given intraperitoneally. A catheter (HAKKO disposable ELASTER TYPE2, 25G×38 mm) filled with heparin-saline solution, connected to a pressure transducer, was inserted into the thoracic aorta and left ventricle (LV) through the right carotid artery to measure aortic pressure and LV pressure. Mean arterial pressure, LV pressure, LV dp/dt, LV −dp/dt, and heart rate were recorded using a polygraph system (Nihon Kohden). A blood sample (1.5 ml) was then collected from the carotid arterial catheter for measuring plasma NE. The rats were then killed and their hearts, lungs, livers, and left stellate ganglia were removed. Each heart (LV + septum), lung, and liver was weighted. To establish mice that selectively expressed enhanced green fluorescent protein (EGFP) in sympathetic nerves, mice carrying a reporter gene construct chicken β-actin promoter (CAG)-chloramphenicol acetyl transferase (CAT)-EGFP (Kawamoto et al., 2000) were crossed with a mouse line expressing Cre recombinase under the control of the dopamine β-hydroxylase (DBH) promoter (Matsushita et al., 2004). The CAG-CAT EGFP transgenic mouse was a gift from J. Miyazaki (Osaka University, Osaka, Japan). The DBH-Cre recombinase transgenic mouse was provided by K. Kobayashi (Fukushima Medical University, Fukushima, Japan). Five-week-old DBH-Cre/Floxed-EGFP mice were implanted osmotic mini pumps (ALZET Osmotic Pumps, model 2004) into the interscapular region under above-mentioned anesthesia. NE was infused at a rate of 0.05 mg/kg/hr for maximum 28 days. Vehicle-infusion mice were used as controls. The animals were killed at 28-day after implantation of osmotic pumps. All animal experiments approved by the Animal Care and Use Committee of the Keio University.

2.2. Plasma NE measurement

Blood samples were collected in iced heparin-treated tubes containing EDTA-2Na (1 mg/ml) and centrifuged (500×g) at 4 °C for 10 min. Plasma was aliquoted and stored at -20 °C until subsequent assay. NE was assayed by high-performance liquid chromatography (HPLC) with electrochemical detection as described previously (Hjemdahl, 1984).

2.3. Tissue NE measurement

Tissue samples were homogenized within 30 sec in 0.1 N HCl containing 0.1% sodium pyrosulfite (Na2S2O5). After centrifugation (10000 g, 30 min), NE was extracted with alumina and determined by HPLC.

2.4. RNA extraction and poly(A)$^+$RNA Northern Blot Analysis

Total RNA from frozen rat tissue samples (LV + septum) was extracted using TRIzol Reagent (GIBCO BRL), and poly(A)$^+$RNA was isolated. Rat NGF, BNP, and glyceraldehyde-3-phosphate dehydrogenase (GAPDH) cDNA were obtained by RT-PCR from the heart and cloned into the pCRα plasmid. GAPDH cDNA was used as an internal control. Inserts were labeled with [α-^{32}P]dCTP by the random priming technique. A 2.5 μg sample of poly(A)$^+$RNA was run on a 1% MOPS/formaldehyde-agarose gel, and Northern blots were performed as described previously (Sano et al., 2000).

2.5. Immunohistochemical procedures

Sample fixation, embedding, sectioning, and blocking were as described previously (Mabe et al., 2006). To detect nerve fibers in the heart, frozen sections were incubated with double antibodies against protein gene product 9.5 (PGP9.5) (Ultraclone UK, RA95101; 1:2000), growth-associated protein (GAP43) (CHEMICON, AB5220; 1:4000), tyrosine hydroxylase (TH) (CHEMICON, AB152; 1:200), or GFP (Medical&Biological Laboratories, 598; 1:500) and α-Actinin (Sigma, A7811; 1:800). The following secondary antibodies were used: Alexa Fluor 488-conjugated donkky anti-rabbit IgG (Molecular Probes; 1:200), polyclonal swine anti-rabbit TRITC (DAKO; 1:200), Alexa Fluor

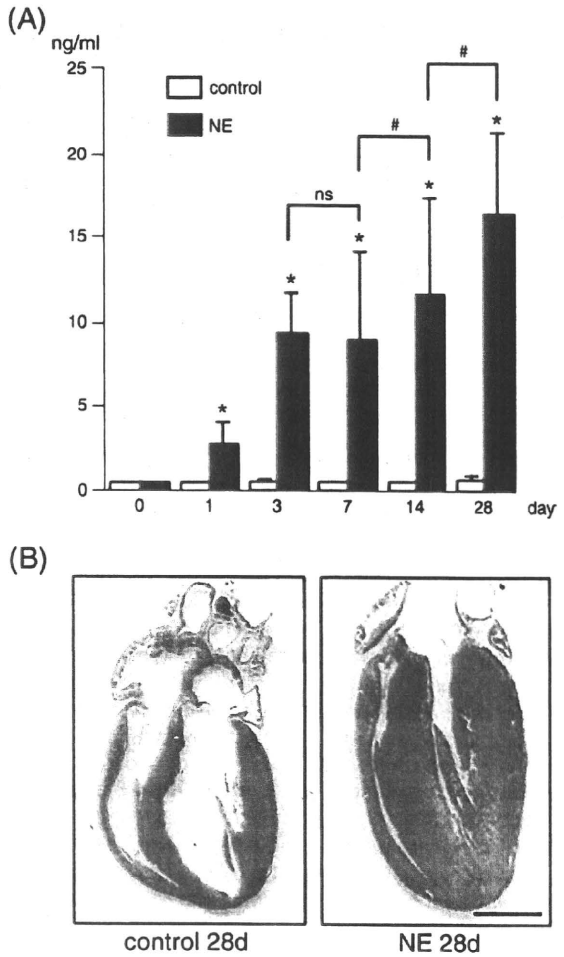

Fig. 1. (A) Plasma concentrations of NE in control and NE-exposed rat. *p<0.01 compared to control at same day, #p<0.01, ns: not significant. (B) Representative section along the long-axis of heart from control and NE-exposed rats at 28-day stained by HE. Note that the LV is markedly thickened and the LV cavity is narrowed. Scale bar indicates 4 mm.

Table 1
Mean wet weight of the tissues in control and NE-treated rats.

	BW (g)	LV + S(mg)	LV + S /body weight (10^{-3})	Lung(mg)	Lung /body weight (10^{-3})	Liver(mg)	Liver /body weight (10^{-3})
Day 0							
Control (n = 7)	248 ± 9	565 ± 49	2.3 ± 0.3	1178 ± 226	4.8 ± 0.4	8320 ± 149	33.5 ± 0.8
NE (n = 8)	259 ± 11	549 ± 25	2.1 ± 0.1	1184 ± 88	4.6 ± 0.7	8470 ± 135	32.7 ± 0.8
Day 1							
Control (n = 8)	245 ± 9	569 ± 17	2.4 ± 0.1	1154 ± 154	4.7 ± 0.7	8286 ± 136	33.8 ± 0.8
NE (n = 14)	254 ± 13	571 ± 38	2.3 ± 0.1	1163 ± 115	4.6 ± 0.9	8433 ± 457	33.2 ± 1.6
Day 3							
Control (n = 8)	267 ± 8	622 ± 41	2.3 ± 0.1	1195 ± 125	4.5 ± 0.5	8619 ± 195	32.3 ± 1.1
NE (n = 15)	258 ± 12	647 ± 64	2.6 ± 0.3	1173 ± 271	4.5 ± 0.5	8590 ± 223	33.3 ± 1.7
Day 7							
Control (n = 8)	273 ± 11	635 ± 17	2.3 ± 0.1	1243 ± 221	4.5 ± 0.6	8872 ± 123	32.5 ± 0.9
NE (n = 12)	267 ± 12	782 ± 72*	2.9 ± 0.3*	1287 ± 169	4.8 ± 0.6	8663 ± 198	32.4 ± 2.2
Day 14							
Control (n = 8)	289 ± 10	638 ± 41	2.2 ± 0.1	1397 ± 153	4.8 ± 0.7	8940 ± 114	30.9 ± 0.4
NE (n = 13)	270 ± 18	862 ± 97*	3.1 ± 0.3*	1375 ± 224	5.1 ± 0.4	8897 ± 251	33.0 ± 1.7
Day 28							
Control (n = 8)	306 ± 13	710 ± 16	2.3 ± 0.1	1473 ± 246	4.8 ± 0.8	9117 ± 108	29.8 ± 0.4
NE (n = 20)	317 ± 21	983 ± 88*	3.2 ± 0.2*	1538 ± 184	4.8 ± 0.9	9430 ± 322	28.8 ± 2.5

*: p 0.01 vs. control.

488-conjugated goat anti-mouse IgG (Molecular Probes; 1:200), and Alexa Fluor 546-conjugated goat anti-mouse IgG (Molecular Probes; 1:200). Apoptosis was measured by using a TUNEL assay kit (Promega). The samples were observed under a Zeiss LSM 510 META confocal microcopy (Germany). Immunostained areas were quantified using NIH image, as described previously (Cao et al., 2000).

2.6. Statistics

Values are presented as means ± SD. The significance of differences among mean values was determined by ANOVA. Statistical comparison of the control group with treated group was carried out using the non-parametric Fisher's multiple comparison tests. The level accepted for significance was $p<0.05$.

3. Results

3.1. Plasma NE concentration

To begin with, to address the characterization of continuous NE infusion model, we measured the plasma NE concentration in the control and NE infusion rats. Plasma NE concentration in NE-treated rats was significantly increased from 1-day after administration compared with control rats. Although the plasma NE level once reached a plateau at around 9 ng/ml between 3-and 7-day, it started to increase after that and finally reached to 16.1 ± 5.6 ng/ml at 28-day (control level was 0.39 ± 0.1 ng/ml, $p<0.01$) (Fig. 1A).

Table 2
Hemodynamic measurements.

	Mean BP (mmHg)	LVEDP (mmHg)	dP/dt (mmHg / sec)	-dP/dt (mmHg / sec)	HR (bpm)
Day 0					
Control (n = 7)	112 ± 4	2.5 ± 0.6	9410 ± 529	6133 ± 643	316 ± 16
NE (n = 8)	103 ± 6	2.9 ± 0.5	9267 ± 416	6318 ± 306	306 ± 24
Day 1					
Control (n = 8)	114 ± 15	3.0 ± 0.6	9333 ± 503	6267 ± 416	316 ± 17
NE (n = 14)	123 ± 9	3.0 ± 0.6	9250 ± 632	6105 ± 469	332 ± 25
Day 3					
Control (n = 8)	118 ± 6	3.1 ± 0.5	9366 ± 423	5917 ± 402	324 ± 30
NE (n = 15)	125 ± 21	5.5 ± 1.4	9467 ± 372	6334 ± 501	339 ± 31
Day 7					
Control (n = 8)	108 ± 16	2.9 ± 0.4	9067 ± 306	5967 ± 153	311 ± 9
NE (n = 12)	127 ± 10	6.7 ± 1.2*	8120 ± 415	5114 ± 458	343 ± 32
Day 14					
Control (n = 8)	103 ± 3	2.9 ± 0.5	9305 ± 436	5907 ± 265	311 ± 9
NE (n = 13)	131 ± 23*	7.9 ± 1.5*	6114 ± 460*	4771 ± 594	349 ± 25
Day 28					
Control (n = 8)	110 ± 4	3.4 ± 0.6	9467 ± 416	6008 ± 296	316 ± 17
NE (n = 20)	143 ± 19*	15 ± 1.9*	5843 ± 476*	3729 ± 419*	360 ± 20*

*: p 0.01 vs. control.

3.2. Appearance and weights

The representative photograph of the longitudinal section of the whole heart in the control and NE-treated rats at 28-day were shown in Fig. 1B. Left ventricular (LV) wall was markedly thickened, and LV cavity was narrowed. Right ventricular free wall was also thickened compared with the control, but less conspicuous than LV. Then, the whole body, LV free wall with septum (S) (LV + S), lung, and liver were separately weighed, and were shown in Table 1. The ratio of LV + S/body weight

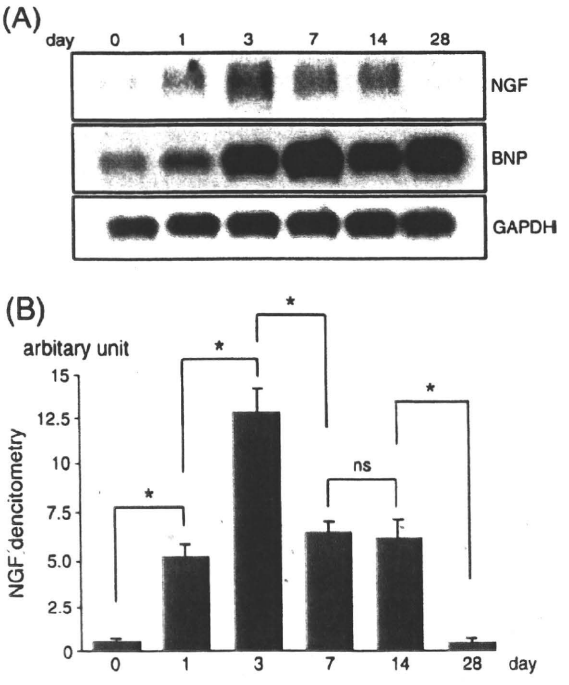

Fig. 2. (A) Northern blot analysis of NGF, BNP, and GAPDH in the left ventricle of NE-exposed rats. (B) Dencitometry analysis of NGF mRNA expression. Northern blot analysis was repeated three times. Expression of NGF mRNA was upregulated at 3-day, subsequently downregulated, and finally almost disappeared at 28-day. *$p<0.01$, ns: not significant.

(BW) increased from 7-day, and reached by 1.39-fold of the control rats at 28-day. NE-treated rats at-28 day had pleural effusion and ascites. This was the reason why the BW of NE-treated rats at 28- day turned to increase, although those at 14-day decreased compared with control. That was also the cause of unchanged ratio of lung/BW and liver/BW between two groups at 28-day, whereas both lung and liver weight themselves in NE-treated rats were increased. Similarly, the ratio of LV + S/BW in NE-treated rats at 28-day should be much greater than that of controls. These findings indicated that NE treatment for 28 days induced decompensated LV hypertrophy (LVH).

3.3. Hemodynamic measurements

Mean blood pressure of NE-treated rats began to increase at 1-day after NE exposure, significantly increased at 14-day, and reached at 143 ± 19 mmHg (control; 110 ± 4 mmHg) at 28-day (Table 2). LV end-diastolic

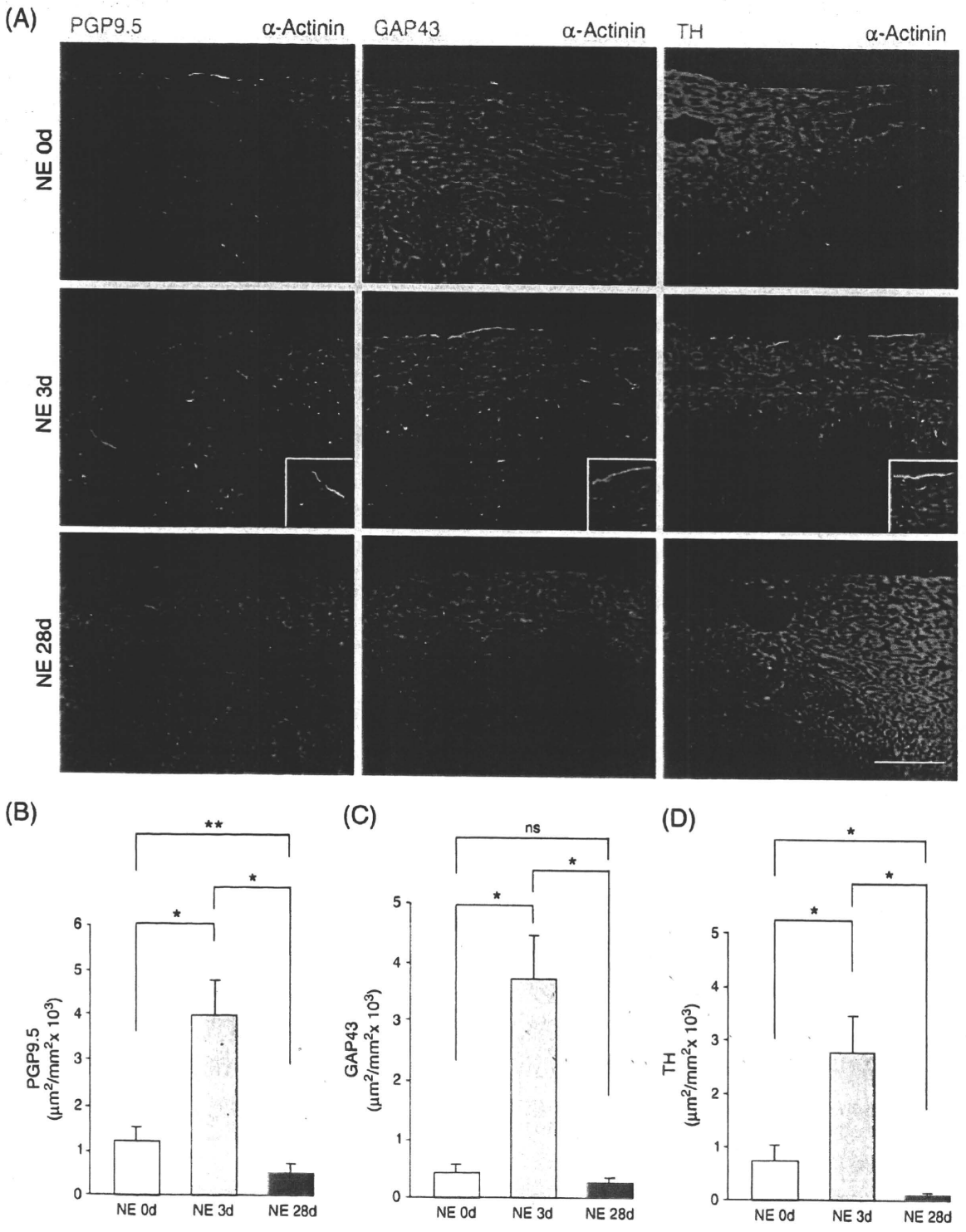

Fig. 3. (A) Double-immunofluorescent staining for PGP9.5, GAP43, and TH with α-Actinin in the LV of 0-, 3-, and 28-day after NE infusion. Insets show high magnification of each sample. (B, C, D) Quantitative analysis of the immunostained area for PGP9.5 (B), GAP43 (C), and TH (D). Scale bar indicates 200 μm. *$p<0.01$, **$p<0.05$, ns: not significant.

pressure (LVEDP) of NE-treated rats started to be raised at 3-day and markedly increased up to 15 ± 1.9 mmHg (control; 3.4 ± 0.6 mmHg) at 28-day. Although it was not significant, it was noteworthy that both dP/dt and |−dP/dt| were temporally elevated in NE-exposed rats at 3-day, whereas these were significantly attenuated at 14-day. Heart rates in NE-infused rats were significantly higher than control at 28-day. These data indicated that NE treatment for 28 days induced heart failure model caused by pressure-overload and/or catecholamine injury.

3.4. NGF and BNP mRNA expression in LV

The performance of NGF mRNA expression in LV of NE-infused rats was immensely unique. In briefly, NGF mRNA was prominently augmented at 3-day after exposure of NE, and after that, it was down-regulated and almost completely disappeared at 28-day. It showed biphasic change through the 28 days. On the other hand, BNP mRNA expression was predictably increased proportionally with the augmentation of LVEDP (Fig. 2 and Table 2).

3.5. Immunohistochemistory for nerve density in heart section

Levels of NGF expression within innervated tissue roughly correspond to innervation density. Thus, we performed an immunohistochemical staining of protein gene product 9.5 (PGP9.5), growth associated protein 43 (GAP43) and tyrosine hydroxylase (TH) to evaluate the nerve density. The PGP9 5 is specifically expressed in nerve fiber axon. GAP43 is a protein that was expressed when the nerve terminal develops. TH is an enzyme that catalyzes the conversion of L-tyrosine to L-DOPA and is a rate-determining enzyme for catecholamine synthesis. For this reason, it is used as a marker of sympathetic nerves. Interestingly, there was a remarkable increase in the expression of PGP9.5, GAP43, and TH in the LV at 3-day after administration of NE. Newly developed nerves were prominent at the

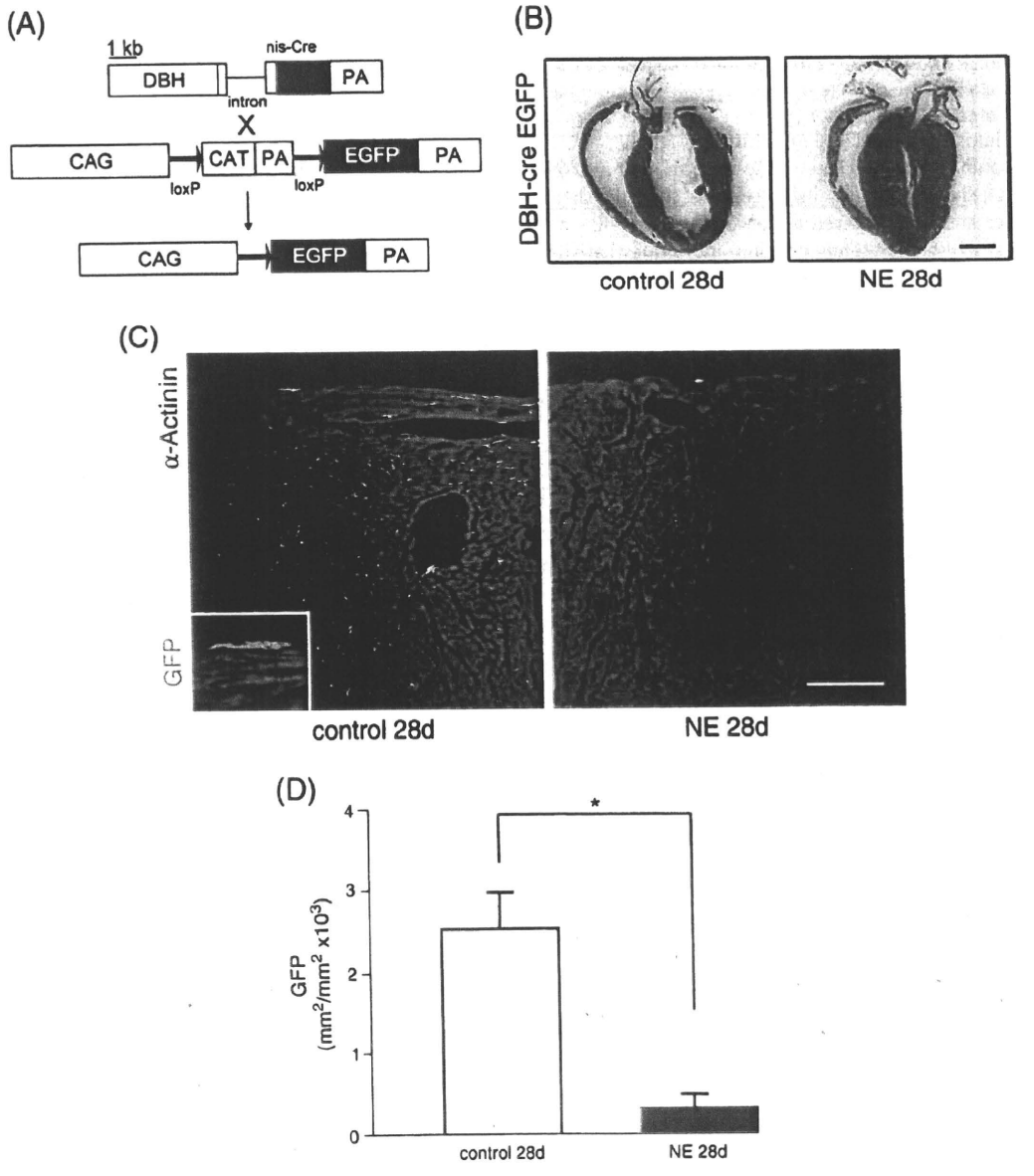

Fig. 4. (A) Dopamine β-hydroxylase (DBH)-Cre transgenic mice were crossed with CAG-CAT-EGFP mice. In the double-transgenic mice ($Cre^+/EGFP^+$), Cre-loxP recombination deletes the CAT gene cassette, leading to the expression of EGFP in sympathetic neurons. (B) Representative section of heart along the long axis from control and NE-infused mice (28-day) stained by HE. Scale bar indicates 2 mm. (C) Double- immunofluorescent staining for GFP and α-Actinin in the LV of control and NE-infused mice at 28-day. Inset shows high magnification. Scale bar indicates 200 μm. (D) Quantitative analysis of the immunostained area for GFP in the LV of control and NE-infused mice. *$p<0.01$.

epicardial layer or the perivascular area, indicated sympathetic neurons (Fig. 3A). The quantitative analysis revealed that PGP9.5, GAP43, and TH increased 3.2-fold, 9.1-fold, and 3.8-fold respectively, in LV at 3-day after NE administration compared with 0-day. (Fig. 3B, C, D). In contrast, not only growth cone marker GAP43 -immunostained neurons, but also nerve fiber marker PGP9.5-immunostained neurons were conspicuously down-regulated in decompensated hypertrophic LV at 28-day (Fig. 3A). The quantitative analysis revealed that the immunostained area of PGP9.5 and TH at 28-day decreased by 88% and 95%, respectively of that at 3-day and also decreased by 58% and 88%, respectively of that at 0 day. The immunostained area of GAP43 at 28-day down-regulated by 92% of that at 3- day, but there was no significant difference between 0-day and 28-day (Fig. 3B, C). These data indicated that sympathetic nerve density in LV was directly correlated with the NGF expression.

3.6. Cardiac sympathetic nerve density in NE-infused mice using the Cre-LoxP system

To confirm whether cardiac sympathetic nerve density is truly attenuated by long-time exposure of NE, we next prepared double-transgenic conditional knockouts by crossing mice carrying a floxed CAT- CAG- EGFP allele with mice that expressed Cre recombinase under the control of the DBH promoter (Fig. 4A), and subjected them to continuous NE infusion to induce heart failure. The adrenergic cells of brain, adrenal, and stellate ganglia in these mice showed a strong GFP signal (data not shown). Longitudinal sections of the whole heart in NE-infused mice at 28-day showed a marked LVH (Fig. 4B). NE-treated mice at 28-day had systemic effusion, indicating that they were in the decompensated stage of heart failure. Immunostaining revealed that GFP signal were markedly decreased in the LV in NE-injected mice at 28-day (Fig. 4C), with the positively stained areas for GFP in the LV following NE-infusion decreased by 87% compared to controls (Fig. 4D). These data confirmed that long-term NE administration causes the anatomical cardiac sympathetic denervation concomitant with severe heart failure.

3.7. Tissue NE content in LV

The NE that is present in the heart is located in the sympathetic nerve fibers rather than in the myocardium per se. To investigate the alteration of sympathetic nerve density could correspond to the sympathetic terminal NE stores, we measured the NE content of the LV tissue in the control and NE-exposed rats. The NE content at 3-day in the LV of the NE-exposed rats tremendously increased 2.1-fold compared with the control at 3- day, sequentially down-regulated, and markedly decreased at 28-day (Fig. 5). These data indicated that the NGF-dependent sympathetic innervation greatly influenced the patterning of the tissue NE content in the LV and LV performance estimated by dP/dt and -dP/dt (Fig. 5 and Table 2).

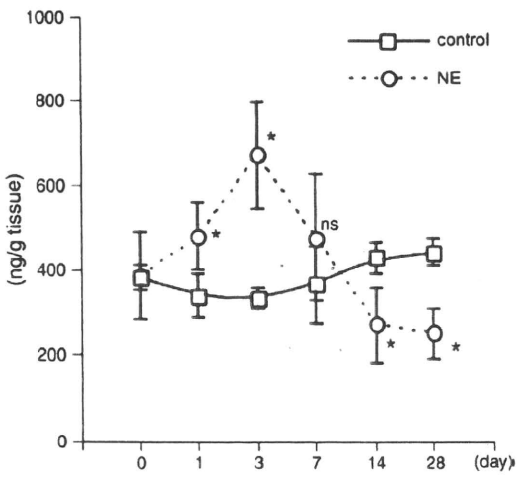

Fig. 5. Tissue NE concentrations in the LV of control and NE-infused rats. *$p<0.01$ compared to control at same day, ns: not significant between control and NE-infused at 7-day.

3.8. Analysis of neuronal cell bodies in stellate ganglion

To investigate whether NE-toxicity directly affects the apoptosis of sympathetic nerve cell body in stellate ganglion, we examine TUNEL assay and count the number of neuronal cell bodies at 0-, 3-, and 28-day in NE-infused rats. The small number of TUNEL positive cells was only observed in the interstitial cells, but not in the neuronal cell bodies at either 0-, 3-, or 28-day (Fig. 6A). Moreover, the number of neuronal cell bodies in stellate ganglion was not significantly different among 0-, 3-, and 28-day (Fig. 6B).

4. Discussion

4.1. Character of NE-infusion model

Continuous NE administration by osmotic pump effectively maintained the high plasma NE concentration throughout 28 days in rats. The level of the concentration reached to a plateau at 3-day after exposure, maintaining the level until 7-day, however it seemed to exceed the estimated value at 28-day. It is generally known that in patients with advanced heart failure, the circulating NE concentration is higher than the level found in normal subjects (Meredith et al., 1993). In our model at 28-day, the higher plasma NE level was presumably modified by heart failure, that is to say, NE induced NE release. As evidenced by the retention of pleural effusion and ascites accompanied with weight gain and the prominent increase of LVEDP, the NE- infused rats at 28-day presented decompensated phase of heart failure. The mean blood pressure of NE-infused rats at 28 day was significantly increased, however compared with the other high blood pressure model, e.g. transaortic constriction mouse or Dahl salt sensitive rat, the level was not enough to produce pressure overload induced heart failure (Sheikh et al., 2008; Miyachi et al., 2009). For the reason of these, we estimated the main etiology of cardiomyopathy in this model as a result of NE induced cardiac injury with hypertrophy directly derived from NE.

4.2. Sympathetic hyper-innervation phase towards hypertrophy

The cardiac performance of NE-exposed rats temporally accelerated at 3 day. Around this phase, cardiac muscles were started to be driven by the increasing circulatory NE via β1 adrenergic receptors. Moreover, at that time, we confirmed that NE content in the sympathetic nerve terminal was also upregulated, reasonably accompanied by sympathetic hyperinnervation. Locally released NE from hyperinervated nerve terminals was presumably more effective in controlling cardiac performance than circulatory NE (Chang et al., 1991). Needless to say, NE itself is a strong cardiac hypertrophic factor and it also derives other hypertorphic factors, e.g. endothelin-1(ET-1), angiotensin II, leukemia inhibitory factor (LIF), from cardiomyocytes (Okada et al., 1995; Baker et al., 1990; Wang et al., 2001). Among these factors, ET-1 has been proven as a factor which can induce NGF expression in cardiomyocytes via ET-A receptor/Giβγ pathway (Ieda et al., 2004). In this study, we observed the augmented NGF expression in the LV of NE-infused rat at 3-day. Although we did not examine the expression of ET-1 in this study, we speculated that the augmented expression of NGF was presumably elicited by ET-1. This speculation is strongly supported by the study of Kaddoura et al. They reported that ventricular expression of ET-1 mRNA is elevated in the first 3 days and falls after that in NE-infused rat (Kaddoura et al., 1996). Moreover, we recently reported that the augmented NGF mRNA expression concomitant with upregulated ET-1 mRNA causes cardiac sympathetic hyperinnervation in pressure-